Holocene atmospheric circulation in the central North Pacific: a new terrestrial diatom and $\delta^{18}O$ dataset from the Aleutian Islands

Hannah L Bailey [a,b,c] *, Darrell S Kaufman [d], Hilary J Sloane [e], Alun L Hubbard [f], Andrew CG Henderson [g], Melanie J Leng [e,h], Hanno Meyer [b], and Jeffrey M Welker [a, c]

[a] Department of Biological Sciences, University of Alaska Anchorage, Anchorage, AK 99508, USA

[b] Alfred Wegener Institute for Polar and Marine Research, Potsdam 14473, Germany

[c] Department of Ecology and Genetics, University of Oulu, Oulu, Finland

[d] School of Earth Sciences & Environmental Sustainability, Northern Arizona University, Flagstaff, AZ 86011, USA

[e] NERC Isotope Geosciences Facility, British Geological Survey, Nottingham NG12 5GG, UK

[f] Centre for Arctic Gas Hydrate, Environment and Climate, Department of Geology, UiT The Arctic University of Norway, 9037 Tromsø, Norway

[g] School of Geography, Politics and Sociology, Newcastle University, Newcastle-upon-Tyne, NE7 1RU, UK

[h] Centre for Environmental Geochemistry, School of Biosciences, University of Nottingham, Loughborough, LE12 5RD, UK

* *Corresponding author*. Current address and affiliation: Hannah.Bailey@oulu.fi (University of Oulu)

Key words: Holocene; Paleoclimate; North Pacific; Limnology; Stable Isotopes; Diatoms

Highlights:

- New Holocene oxygen isotope record from the Aleutian Islands
- Diatom $\delta^{18}O$ reflects shifts in synoptic-scale atmospheric circulation
- Warmer/wetter early-mid Holocene, cooler/drier after 4.5 ka
- Enhanced winter circulation corresponds to Holocene glacier advances
- Current environmental changes unprecedented within past 9.6 ka

Abstract

The North Pacific is a zone of cyclogenesis that modulates synoptic-scale atmospheric circulation, yet there is a paucity of instrumental and paleoclimate data to fully constrain its long-term state and variability. We present the first Holocene oxygen isotope record ($\delta^{18}O_{diatom}$) from the Aleutian Islands, using siliceous diatoms preserved in Heart Lake on Adak Island (51.85° N, 176.69° W). This study builds on previous work demonstrating that Heart Lake sedimentary $\delta^{18}O_{diatom}$ values record the $\delta^{18}O$ signal of precipitation, and correlate significantly with atmospheric circulation indices over the past century. We apply this empirical relationship to interpret a new 9.6 ka $\delta^{18}O_{diatom}$ record from the same lake, supported by diatom assemblage analysis. Our results demonstrate distinct shifts in the prevailing trajectory of storm systems that drove spatially heterogeneous patterns of moisture delivery and climate across the region. During the early-mid Holocene, a warmer/wetter climate prevailed due to a predominantly westerly Aleutian Low that enhanced advection of warm ^{18}O-enriched Pacific moisture to Adak, and culminated in a $\delta^{18}O_{diatom}$ maxima (33.3 ‰) at 7.6 ka during the Holocene Thermal Maximum. After 4.5 ka, relatively lower $\delta^{18}O_{diatom}$ indicates cooler/drier conditions associated with enhanced northerly circulation that persisted into the 21st century. Our analysis is consistent with surface climate conditions inferred from a suite of terrestrial and marine climate-proxy records. This new Holocene dataset bridges the gap in an expanding regional network of paleoisotope studies, and provides a fresh assessment of the complex spatial patterns of Holocene climate across Beringia and the atmospheric forces driving them.

1. Introduction

Numerous paleoenvironmental studies now contribute to a global synthesis and understanding of Holocene climate change over the past 11.7 ka [*Mayewski et al*. 2004; *Marcott et al*. 2013; *Rehfeld et al*. 2018]. By comparing common trends between individual proxy records, these studies provide a means to infer the timing, scale, and spatial extent of major Holocene climatic features. These include stepwise climate transitions, intervals exceeding twentieth century warmth, and the low-frequency behaviour and modes of natural climate variability. At broad (i.e. global) spatial and temporal scales these trends are relatively coherent and unambiguous, yet at finer spatial scales, climate variability is more pronounced due to local and regional factors. Such variability is highlighted in two recent paleoclimate syntheses focused on west and eastern Beringia – the region extending from northeast Siberia to northwest Canada (Fig. 1a) [*Brooks et al*. 2015; *Kaufman et al*. 2016]. While general circulation models (GCM) typically emphasise insolation as the key driver of millennial-scale Holocene climate change [*Renssen et al*. 2009], these compilations indicate a more complex and spatially heterogeneous climate evolution than implied by linear insolation forcing alone. For example, major climatic features previously considered ubiquitous, such as a prominent Holocene thermal maximum (HTM) [*Kaufman et al*. 2004], are now recognised to be spatially asynchronous across this vast region [*Kaufman et al*. 2016]. Moreover, existing terrestrial water isotope records are also shown to be ambiguous and contradictory during the Holocene [*Kaufman et al*. 2016], and the most recent suite of model-data comparisons reveal significant mismatches between simulated and reconstructed Holocene temperatures in Alaska [*Zhang et al*. 2017].

At the synoptic scale, Beringia is located within the main centre of influence of the Aleutian Low; one of the most dominant ocean-atmospheric systems in the Northern Hemisphere and of global climate significance [*Rodionov et al*. 2007]. However, virtually all available terrestrial paleoclimate data are restricted to mainland Alaska and eastern Russia

[*Sundqvist et al*. 2014; *Brooks et al*. 2015; *Kaufman et al.* 2016], and compared to lower latitude regions, paleoisotope reconstructions are sparse [*Kaufman et al*. 2016]. This partly reflects a lack of base-line water isotope measurements for constraining the regional water isotope cycle [e.g. *Welker*, 2000; *Anderson et al*. 2016], as well as a paucity of lake core studies with continuous sequences of carbonate-rich sediments – or suitable alternatives − for isotopic analysis. Hence, to elucidate past and future climate in this region, there is an outstanding requirement for greater spatial coverage of highly resolved and accurately dated paleoclimate datasets, as well as an empirical-based understanding of the atmospheric and environmental controls driving them.

To address this, we present the first Holocene oxygen isotope record from the Aleutian Islands in south west Alaska. Our isotope measurements derive from siliceous diatoms ($\delta^{18}O_{diatom}$) preserved in the sediments of Heart Lake, on Adak Island (Fig. 1b), and are supported by diatom assemblage analysis of the same sedimentary sequence. We build on earlier work by *Bailey et al*. [2015] who demonstrate that Heart Lake $\delta^{18}O_{diatom}$ values correlate significantly with North Pacific climate indices over the past hundred years ($r = 0.43$; $p < 0.02$, $n = 28$). Here, we apply this empirically-derived understanding to interpret new $\delta^{18}O_{diatom}$ data from a longer Heart Lake sediment core which extends back to 9.6 ka. The primary aims are to: (1) investigate the forcing and response of this remote region to a warming climate system as it transitioned from the last glacial period; (2) develop a Holocene reconstruction of North Pacific atmospheric circulation; and (3) bridge the gap in the regional network of proxy records to synthesise and assess complex spatio-temporal patterns of natural climate variability across Beringia.

2. Regional Setting

Heart Lake is a small (~0.25 km^2), freshwater through-flow system on Adak Island in the central North Pacific (51.85 ° N, 176.69 ° W) (Fig.1c). The island is volcanic and forms part

106 of the 1900-km-long Aleutian archipelago extending from mainland Alaska to the Russian-
107 Kamchatka Peninsula. The lake watershed area is ~8 km^2 and is situated in low-relief hills
108 surrounded by mountainous terrain (Fig. 1c). There is a single lake basin with a maximum
109 depth of 8 m. One stream inflows from two larger lakes and a small outflow channel drains to
110 the Bering Sea ~2 km to the west. Lake volume is ~8 $\times 10^5$ m^3 and water retention is an
111 estimated two weeks, based on the available stream gauge inflow data [*TDX*, 2013].
112 Inspection of available satellite imagery reveals that Heart Lake freezes over in winter and
113 this ice surface remains into spring [*USGS*, 2017].
114 Adak Island has a mild maritime climate compared to mainland Alaska and is
115 strongly affected by persistent fog and light rain in the summer, and frequent storms and
116 strong winds during winter [*Rodionov et al*. 2007]. Mean annual air temperature is 4.3 °C,
117 and mean winter (December−February) and summer (June−August) values are 1.0 °C and 9.0
118 °C, respectively (1949−2016) [*NOAA*, 2017]. Mean December and July precipitation is 163
119 mm and 71 mm, respectively (Fig. 1d) [*NOAA*, 2017]. Of the total 1.3 m annual precipitation,
120 ~75 % (1.0 m) falls from September to February.
121 The regional climate reflects the configuration of large scale atmospheric−ocean
122 systems, namely the Aleutian Low: a synoptic-scale feature of mean low sea level pressure
123 (SLP) and the leading driver of North Pacific climate [*Mock et al*. 1998]. When the Aleutian
124 Low is 'weak', storms tend to track north over the central Aleutian Islands (Fig. 2a); when
125 the pressure system is 'strong', storms track south of the Aleutians and into the Gulf of
126 Alaska (Fig. 2b) [*Mock et al*. 1998; *Rodionov et al*. 2007]. These circulation patterns vary on
127 interannual to decadal timescales and induce characteristic climate responses that are well
128 expressed in coupled modes of the North Pacific Index (NPI) and the Pacific Decadal
129 Oscillation (PDO) [*Trenberth and Hurrell*, 1994; *Mantua et al*. 1997]. Typically, a strong
130 Aleutian Low (−NPI/+PDO) will induce positive sea surface temperatures (SST), surface air
131 temperatures (SAT), and precipitation anomalies in the Gulf of Alaska and negative

anomalies in the central North Pacific, with contrary conditions during a weak Aleutian Low (+NPI/−PDO) (see Supplementary Fig.1).

3. Materials and Methods

3.1. Sediment and water recovery

Sediment cores and bottom lake water samples were recovered from Heart Lake during the summers of 2009 and 2010. A Garmin GPS sonar was used to survey its bathymetry and revealed a single basin with a maximum depth of 8 m, surrounded by a shallow platform < 2 m deep (see Supplementary Figure 2). Coring sites were selected adjacent to the deepest part of the basin at a depth of 7.6 m. Seven sediment cores were extracted using percussion and hand-held gravity coring devices operated from a floating platform. Bottom lake water samples were collected *in situ* at the sediment-water interface during gravity coring. Following core extraction the water was directly siphoned from the corer and sealed in 50 ml vials, ensuring no head space. Sediment cores were then split lengthways, packaged, and shipped with water samples to Northern Arizona University where they were stored at 4°C until they were sub-sampled and analyzed. Our study focuses on the longest percussion core (10-AS-1D; 5.9 m) and two accompanying surface gravity cores (09-AS-1A, 0.81 m; and 09-AS-1B, 0.44 m). For a detailed description of the sediment core's lithostratigraphy, see *Krawiec et al*. [2013].

3.2. Chronology

The composite age model for 10-AS-1D and 09-AS-1A is presented in a separate paper devoted to the tephrostratigraphy and radiometric dating of the Heart Lake sedimentary sequence [*Krawiec et al*. 2013] (Supplementary Fig. 3a). In summary, a Monte Carlo approach was employed to model the age-depth relation of 16 macrofossil AMS radiocarbon (^{14}C) dates, together with a peak in recent ^{239}+^{240}Pu activity and the age of the sediment-water

interface (2009 AD) [*Krawiec et al*. 2013]. Tephrostratigraphy was used to independently cross check the accuracy of the chronology, whereby the ages of down core tephra horizons from Heart Lake were compared with tephra ages from nearby Andrew Lake and previously published outcrop studies [*Krawiec et al*. 2013]. The chronology for surface core 09-AS-1B derives from radiometric dating of ^{210}Pb, ^{226}Ra, ^{137}Cs and ^{241}Am by direct gamma assay on 14 dried sediment samples from the upper core section [*Bailey et al*. 2015] (Supplementary Fig. 3b). The cores were cross-correlated using a prominent tephra horizon found in all three sedimentary sequences [*Krawiec et al*. 2013; *Bailey et al*. 2015]. All ages herein are expressed as thousands of calendar years (ka) prior to 1950 AD, where 1 ka = 1000 cal yr BP.

3.3. Stable isotope analyses

A total of 147 sediment samples were processed for $\delta^{18}O_{diatom}$ analysis. These samples range in age from 9.6 ka (587 cm depth) to 2009 AD, and are sub-/decadally resolved for the most recent 1500 years and at centennial resolution thereafter. From the 5.9 m-long core 10-AS-1D, 1 cm^3 of sediment was extracted at 7 cm intervals from the base (587 cm) to the top of the core. This was the optimal sampling resolution to avoid tephra layers which could potentially cause contamination issues [*Lamb et al*. 2007]. The surface cores 09-AS-1A and 09-AS-1B were both sampled in contiguous 0.5 cm increments. This detail was used to capture sub-decadal changes in $\delta^{18}O_{diatom}$ over the past century for direct comparison with instrumental datasets [see *Bailey et al*. 2015]

Sediment samples were prepared using a hybrid process of chemical digestion, sieving, and heavy liquid separation adapted from *Morley et al*. [2004]. To remove organic and carbonate material, samples were treated with 30% H_2O_2 at 90°C until reactions ceased, before using 5 % HCl at ambient temperature. Samples were then centrifuged in sodium polytungstate ($3Na_2WO_4 9WO_3.H_2O$) (SPT) heavy liquid at 2500 rpm for 20 minutes, resulting in the separation and suspension of diatoms from the heavier detritus. This

183 procedure was repeated three times for each sample using specific gravities of 2.50, 2.30 and
184 2.25 g ml^{-1}. After the final SPT separation, samples were washed five times in ultrapure water
185 (UPW) at 1500 rpm for 5 minutes and vacuum filtered through a 3 µm cellulose nitrate
186 membrane to remove potential clay minerals and/or broken diatom fragments. The < 3 µm
187 fraction was discarded as it was too small (< 1 mg) to be analyzed and, upon further
188 inspection under a light microscope, contained only small broken diatom fragments and
189 detritus. The remaining samples were treated with a final stage of 30 % H_2O_2 at 60 °C for one
190 week to ensure no traces of organic matter remained.
191 Purified diatom samples were analyzed for $\delta^{18}O_{diatom}$ using the stepwise fluorination
192 method [*Leng and Sloane*, 2008] at the NERC Isotope Geosciences Laboratory in Keyworth,
193 UK. The outer hydrous layer of the diatom was removed in a pre-fluorination stage using a
194 BrF_5 reagent at low temperature [*Leclerc and Labeyrie*, 1987]. This was followed by a full
195 reaction at high temperature to liberate oxygen that was converted to CO_2 [*Clayton and*
196 *Mayeda*, 1963] and measured for $\delta^{18}O_{diatom}$ using a MAT 253 dual-inlet mass spectrometer.
197 Replicate analyses indicate an analytical reproducibility of ±0.19 ‰ (1σ) for the samples, and
198 ±0.30 ‰ (1σ) for the diatom standard BFC_{mod}. All $\delta^{18}O$ values were converted to the Vienna
199 Standard Mean Ocean Water (VSMOW) scale using the BFC_{mod} standard for calibration.
200 Two Heart Lake water samples were measured for their oxygen and hydrogen (δD)
201 isotope composition using a Thermo-Finnigan Deltaplus XL gas mass spectrometer at the
202 Colorado Plateau Stable Isotope Laboratory, Northern Arizona University, USA. Analytical
203 precision on internal working standards was ±0.1 % for $\delta^{18}O$ and ±1 % for δD. All values are
204 reported here in per mil (‰) relative to VSMOW.
205
206 ***3.3.1. Contamination assessment***
207 All purified diatom samples (n = 147) were visually inspected for contamination using an
208 OLYMPUS BX40 light microscope. Thirty samples were selected down-core and further

209 inspected using a Hitachi S-4700 field emission scanning electron microscope (SEM). In
210 addition, fourier transform infrared spectroscopy (FTIR) was applied to assess the chemical
211 composition and sample purity of 16 diatom samples from core 10-AS-1D [*Swann and*
212 *Patwardham*, 2011]. These samples, together with the BFC_{mod} diatom standard, were
213 analyzed using FTIR at the British Geological Survey in Keyworth, UK [*Bailey et al.* 2014].
214 FTIR analyses of all purified diatom isotope samples measured (n=16) indicate peaks
215 corresponding to the BFC_{mod} standard, known to represent clean, fossilised diatomite
216 (Supplementary Fig. 4). Spectral deviation from the standard would indicate additional
217 compounds and contamination by non-diatom components [*Swann and Patwardhan*, 2011];
218 peaks centred at ~450 cm^{-1}, ~800 cm^{-1} and ~1100 cm^{-1} confirm pure silica and the integrity of
219 our diatom isotope samples [*Bailey et al*. 2014].
220
221 **3.4. Diatom assemblage analysis**
222 Fifty-seven sub-samples of the purified diatom material used for $\delta^{18}O_{diatom}$ analysis were
223 retained for diatom species analysis. These include 33 samples selected at *c.* 13 cm intervals
224 from AS-10-1D, and 24 samples at a contiguous 0.5 cm resolution from AS-09-1B. Diatom
225 slides were prepared on a hot plate using Naphrax® mounting medium. A minimum of 300
226 diatom frustules per sample were counted along transects at x1000 magnification, under an
227 OLYMPUS BX40 light microscope. Taxonomic identification was based on classifications in
228 *Camburn and Charles* [2000] and *Krammer and Lange-Bertalot* [1986−1991].
229 Following diatom identification, species counts were converted to percentage
230 abundance and evaluated using the software package Tilia (*v.2.0.41*) [*Grimm*, 2015]. For
231 diatom zone demarcation, a constrained incremental sum-of-squares cluster analysis
232 (CONISS) [*Grimm*, 1987] was applied to all dominant taxa with a relative abundance >5 %
233 in at least one sample. To quantitatively assess the down core trends in diatom assemblages, a
234 principal components analysis (PCA) [*ter Braak and Prentice*, 1988] was applied to a

correlation matrix based on the dominant (>5 %) diatom species in all 57 samples. The analysis was performed on untransformed percentage data using the program C2 (*v.1.7.6*) [*Juggins*, 2014].

4. Results

4.1. Diatom flora

Diatom frustules are well preserved in all samples and show no sign of valve dissolution. The flora is diverse and a total of 155 different freshwater diatom species were identified. Of these, 11 species account for > 90 % of all diatoms present in all samples. These include species belonging to the genera *Aulacoseira*, *Cyclotella*, *Rossithidium*, and small fragilarioid taxa (consisting of the genera *Fragilaria*, *Pseudostaurosira*, *Staurosira*, *Stauroforma*, and *Staurosirella*). Species with an abundance ≥ 5 % in at least one stratigraphic level are presented (Fig. 3), and the record is divided into four zones based on the CONISS dendrogram: *Zone 1* (9.6−8.6 ka; 587−452 cm), *Zone 2* (8.6−4.4 ka; 452−352 cm), *Zone 3* (4.4 ka−1860 AD; 352−13.25 cm), and *Zone 4* (1860−2009 AD; 13.25−0 cm). Species are grouped into one of three habitat types (planktonic, benthic, or facultatively planktonic) based on classifications by *Spaulding et al*. [2017] (Fig. 3).

Diatom Zone 1 *(587−452 cm; ca. 9.6−8.6 ka)* is dominated by *Staurosirella pinnata* (33 %), *Cyclotella ocellata* (18 %), and other small fragilarioid taxa (60 %) (Fig. 3). By *ca*. 9.0 ka the abundance of *S. pinnata* decreases to 10 % and the planktonic species *Cyclotella rossii* (10−30 %), *Aulacoseira subarctica* (4−25 %) and *Cyclotella ocellata* (5−14 %) are more dominant. Some of the small benthic species all show slight increases in abundance at this time, including *Psammothidium levanderi* (9 %) and *Achnanthidium minutissimum* (6%), albeit at a low relative abundance.

In Zone 2 *(452−352 cm; ca. 8.6−4.4 ka)* the planktonic species *C. ocellata*, *A. subarctica*, and *C.* rossii begin to dominate the assemblage (Fig. 3). Collectively these

species reach a maximum abundance of 75 % between 8.5−7.6 ka; a time when small benthic and facultatively planktonic taxa are at their overall lowest Holocene abundances (0−5 %). Increases in abundances of *Rossithidium pussilum* and other small fragilarioid taxa occur *ca*. 7.6 and 6.8 ka, concurrent with a decrease in planktonic taxa (Fig. 3). After *ca*. 5.0 ka, the abundance of planktonic species gradually decrease, paralleled by increasing abundance of facultatively planktonic taxa.

At the onset of Zone 3 (*352−13.25 cm; 4.4 ka−1860 AD*) a large increase in the facultatively planktonic taxa is paralleled by declines in planktonic taxa (Fig. 3). Collectively, the small fragilarioid taxa make up ~80 % of the assemblages in this zone and several species attain their maximum Holocene abundance, including *S. pinnata* at 4.2 ka (39 %) and *Staurosira construens* at 3.8 ka (28 %). In contrast, planktonic species decline from a mean abundance of 55 % in Zone 2, to 5 % in Zone 3. Only *Tabellaria flocculosa* shows relatively little change in abundance from Zone 2, remaining at ~4%. Of the benthic taxa, *Stauroforma exiguiformis* and *R. pusillum* are also present in high abundances throughout Zone 3, with the former attaining a maximum Holocene abundance of 26 % at *ca*. 2.2 ka.

In Zone 4 (*13.25−0 cm; ca. 1860−2009 AD*) the small fragilarioid taxa continue to dominate the assemblage, comprising ~75 % of the total assemblage *ca*. 1910 AD (Fig. 3). After this time, the abundance of facultatively planktonic taxa steadily decreases as the benthic and planktonic species increase. After *ca*. 1970 AD, the numbers of *A. subarctica* decreases substantially, such that only a few individual frustules were counted per sample.

Stratigraphic changes in diatom flora are captured in the first two PCA components, which collectively account for 71 % of the total assemblage variance (Fig. 4). Additional eigenvectors defined by the PCA (3−5) were not considered given they explain progressively lower proportions of the total variance (λ_3= 0.108, λ_4=0.059, λ_5=0.038). PCA 1 represents 57 % of total variance and correlates to the planktonic species at the positive extreme, and the facultatively planktonic species at the negative extreme. PCA 2 accounts for 14 % of total

287 variance, and correlates to the small fragilarioid taxa (Fig. 4). The Holocene succession of
288 diatom communities in Heart Lake is further illustrated by the time-series of the 54 sample
289 scores on PCA axis 1 (Fig. 3).
290
291 **4.2. Oxygen isotopes**
292 Holocene $\delta^{18}O_{diatom}$ values vary between 24.6 ‰ (1805 AD) and 33.3 ‰ (7.6 ka) ($\bar{x}$ = 29.7
293 ‰, n = 137) (Fig. 5) with a range of ±8.7 ‰ that is appreciably greater than the standard
294 deviation of all samples (±0.19 ‰) and diatom standards (±0.30 ‰) measured. The base of
295 the Heart Lake sediment core has a $\delta^{18}O_{diatom}$ value of 29.7 ‰ at 9.6 ka, and values steadily
296 increase to the maximum Holocene value of 33.3 ‰ at *ca*. 7.6 ka (Fig. 5). After 4.9 ka
297 $\delta^{18}O_{diatom}$ becomes progressively lower until *ca*. 3.5 ka (27.8 ‰) where values remain stable
298 at ~29−30 ‰ until *ca*. 1.0 ka. After *ca*. 1.0 ka, $\delta^{18}O_{diatom}$ exhibits high variability to lower
299 values *ca*. 1250−1340 AD and 1430−1525 AD, and after 1640 AD there is a shift to overall
300 lower $\delta^{18}O_{diatom}$ values, including the Holocene minimum $\delta^{18}O_{diatom}$ value of 24.6 ‰ at 1805
301 AD. The $\delta^{18}O_{diatom}$ values then slightly increase between 1805−1903 AD, before decreasing
302 to the present day (29.8 ‰) (Fig. 5). Using the sub-division age of 4.2 ka for the mid-late
303 Holocene boundary [*Walker et al*. 2012], late Holocene $\delta^{18}O_{diatom}$ is significantly ($p < 0.001$)
304 lower than in the early−mid Holocene.
305
306 **5. Discussion**
307 **5.1. Oxygen isotope paleohydrology and paleoclimatology**
308 Oxygen isotope ratios measured in precipitation ($\delta^{18}O_P$) at Adak airport (1962−67, 1972−73;
309 n = 60) indicate mean annual precipitation-weighted $\delta^{18}O_P$ is −8.8 ‰, with small seasonal
310 differences between January (–9.4 ‰) and July (–8.9 ‰) [*IAEA/WMO*, 2017]. The
311 correspondence between Heart Lake water $\delta^{18}O$ and the local and global meteoric water lines
312 confirms that (1) Heart Lake water $\delta^{18}O$ reflects local precipitation, and (2) evaporative

313 effects influencing precipitation and lake water $\delta^{18}O$ are minimal with no isotopic enrichment
314 (Fig. 6). Specifically, the two Heart Lake bottom water ($\delta^{18}O_{water}$) samples collected in
315 summer 2009 and 2010 ($\bar{x}$ = –9.5 ‰) are directly comparable, within error, to the long term
316 winter and spring $\delta^{18}O_P$ values from Adak airport. These data indicate the lake water budget
317 is dominated by winter and spring precipitation (i.e. snowfall and melt) similar to many lakes
318 and streams across Alaska [*Clegg and Hu*, 2010; *Lachniet et al*. 2016; *Vachula et al*. 2017].
319 There is no correlation between mean monthly $\delta^{18}O_P$ and SAT (r = 0.15, n = 72) or
320 precipitation amount (r = 0.03, n = 72) at Adak airport. Instead, *Bailey et al*. [2015] found
321 that Adak Island $\delta^{18}O_P$ values are primarily controlled by the moisture source and trajectory
322 of local precipitating storm systems. Specifically, winters with intensified Aleutian Low
323 circulation are characterized by precipitation with significantly ($p < 0.05$) lower than mean
324 $\delta^{18}O_P$ values. These variations are explained by systematic shifts in the central foci of the
325 Aleutian Low; when the SLP minimum is near Adak (strong Aleutian Low), polar air masses
326 are drawn south and advect water vapor and precipitation that is relatively depleted in ^{18}O,
327 along with lower-than-average winter temperatures and increased snowfall (Fig. 2b)
328 [*Rodionov et al*. 2007; *Bailey et al*. 2015]. In contrast, a weakened and westerly displaced
329 Aleutian Low increases the southerly Pacific moisture flux to Adak via an enhanced south-
330 westerly storm track (Fig. 2a) [*Rodionov et al*. 2007]. These systems carry warm ^{18}O-
331 enriched moisture, and bring higher-than-average temperatures and increased precipitation to
332 Adak Island [*Bailey et al*. 2015].
333 $\delta^{18}O_{diatom}$ is controlled by several environmental parameters which depend on local
334 hydrology, climate, and the seasonality of diatom growth [*Barker et al*. 2001; *Rioual et al*.
335 2001; *Jones et al*. 2004; *Rosqvist et al*. 2004; *Leng and Barker*, 2006; *Schiff et al*. 2009;
336 *Mackay et al*. 2011; *Meyer et al*. 2015; *Chapligin et al*. 2016]. Previous work by *Bailey et al*.
337 [2015] showed that the surface core $\delta^{18}O_{diatom}$ record from Heart Lake correlates significantly
338 with the winter NPI during the instrumental period (1900−2009 AD) (r = 0.43, $p < 0.02$, n =

28). This positive relationship confirms that Heart Lake diatoms precipitate their silica frustule in isotopic equilibrium with the lake water in which they grow [*Labeyrie*, 1974; *Leclerc and Labeyrie*, 1987], independent of size or species-related vital effects [*Bailey et al.* 2014]. During the spring thaw, it is evident that winter season precipitation ($\delta^{18}O_P$) enters Heart Lake coincident with onset of the spring diatom bloom. A limited component of residual summer growth might be expected, but bulk $\delta^{18}O_{diatom}$ analysis is weighted toward the main period of diatom growth in spring [*Leng et al*. 2001; *Bailey et al*. 2014]. Under the assumption that similar climatic controls on $\delta^{18}O_P$ prevailed before 1900 AD, we use this extended $\delta^{18}O_{diatom}$ record as a proxy for atmospheric circulation throughout the Holocene.

5.2. Holocene environmental history of Adak Island

5.2.1. Early-mid Holocene, 9.6 – 4.4 ka

Adak Island, along with the Aleutian chain, was glaciated during the last glacial maximum, though there are few chronological constraints on the onset and pattern of ice retreat [*Coats*, 1956; *Bradley*, 1948; *Fraser and Snyder*, 1959; *Black*, 1976]. At Heart Lake, percussion coring ceased at a depth of 587 cm without penetrating bedrock or till, indicating the catchment deglaciated prior to 9.6 ka.

From 9.6−9.0 ka, the dominance of fragilarioid and other small benthic taxa reflect a temperate oligotrophic shallow lake with an extensive littoral zone. These pioneering taxa dominate polar to subpolar and mountainous tundra lakes [*Lotter and Bigler*, 2000; *Rühland et al*. 2003; *Hausmann and Pienitz*, 2009; *Devlin and Finkelstein*, 2011] and their presence suggests a relatively short growth season with cool air temperatures [*Smol et al*. 2005; *Rühland et al*. 2008; *Hausmann and Pienitz*, 2009]. Cool/dry conditions at this time are further supported by low concentrations of biogenic silica (BSi) and organic matter (OM) in

363 nearby Andrew Lake [*Krawiec and Kaufman*, 2014] and the dominance of *Salix* and
364 *Empetrum* in northern Adak [*Heusser*, 1978].
365 Heart Lake was increasingly colonized by planktonic diatoms between 9.3−4.4 ka
366 (Fig. 3). Of these, *A. subarctica* is common across Arctic and subarctic zones, and typically
367 shows pronounced periodicity with the spring maximum in non-stratified lakes [*Bradbury et*
368 *al*. 2002; *Baier et al*. 2004; *Rioual et al*. 2007; *Gibson et al*. 2003; *Solovieva et al*. 2015]. It is
369 a heavily silicified species, forming colonies that require turbulence-induced suspension to
370 remain within the photic zone [*Rühland et al*. 2008; *Lotter et al*. 2010], and indicates
371 persistent strong seasonal winds, together with associated turbulent water mixing and nutrient
372 upwelling [*Wang et al*. 2008; *Andrén et al*. 2015; *Solovieva et al*. 2015]. In contrast,
373 *Cyclotella* species have a competitive advantage over the heavily silicified *A. subarctica*
374 during strong stratification [*Andrén et al*. 2015] and typically bloom after ice-out in subarctic
375 regions [*Rühland et al*. 2008; *Hoff et al*. 2015]. In Kamchatka, *Cyclotella* spp. prosper during
376 warmer years [*Lepskaya et al*. 2010], and are broadly considered warm water indicators due
377 to their recent expansion across Arctic lakes [*Smol et al*. 2005; *Rühland et al*. 2008].
378 Collectively, these early-mid Holocene diatom assemblages reveal a phase of overall high
379 lake mixing and turbidity, reduced lake ice cover, and relatively high Si/P ratios [*Interlandi et*
380 *al*. 1999; *Rühland et al*. 2003; *Rioual et al*. 2007]. These changes are further summarized by
381 the Holocene time series of PCA 1 sample scores (Fig. 3).
382 The isotope composition of Heart Lake water was significantly ($p < 0.001$) higher
383 during the early-mid Holocene compared to the late Holocene (Fig. 5), reflecting the
384 prevalence of southerly storms delivering abundant precipitation with higher $\delta^{18}O$ values
385 [*Bailey et al*. 2015]. Such warm, southerly winter storms would promote turbulent mixing
386 and limit the development of winter lake ice, thereby extending the open-water growing
387 season and allowing for a spring diatom assemblage dominated by planktonic species (Fig.
388 3). *Aulacoseira subarctica*, in particular, is abundant in modern lake systems during years

with short, warm winters [*Gibson et al*. 2003; *Horn et al*. 2011]. Elevated pollen percentages of *Cyperaceae* and other wetland species in northern Adak also imply warm/wet conditions at this time [*Heusser*, 1978] and correspond to higher local lake levels prior to 4.0 ka [*Krawiec and Kaufman*, 2014]. Peak $\delta^{18}O_{diatom}$ (33.3 ‰) suggests maximum Holocene warmth at 7.6 ka, an inference supported by the simultaneous maximum Holocene abundance of the warm water indicator *C. occellata* [*Rühland et al*. 2008] (Fig. 3).

The $\delta^{18}O_{diatom}$ record correlates positively with the time series of PCA 1 scores (r = 0.48, $p < 0.001$) and demonstrates that diatom community structure is indirectly connected to climate over millennial timescales. It also indicates that diatom species changes are a natural ecological response to climatically-driven shifts in lake water $\delta^{18}O$, as reflected in the $\delta^{18}O_{diatom}$ record, rather than the converse (i.e. changes in diatom species drive $\delta^{18}O_{diatom}$ variation).

5.2.2. Mid-late Holocene, 4.4 ka – present

At around 4.4 ka, a major shift in diatom composition occurred with marked changes from a predominantly planktonic assemblage to the dominance of small fragilarioid and benthic taxa (Fig. 3). During this transition the relatively warm, deep, and well-mixed open-water conditions of the early-mid Holocene (9.6−4.4 ka) gave way to a less turbulent, potentially shallower lake. This transition coincides with a shift to lower $\delta^{18}O_{diatom}$ values in the late Holocene, reflecting an increase of isotopically depleted water (i.e. snow and/or ice melt) during the spring thaw [*Bailey et al.*, 2015; *Streletskiy et al*. 2015], and reduced warm, ^{18}O-enriched southerly storms that characterized the early-mid Holocene.

An increase in northerly winds and lower temperatures during the late Holocene would have enhanced formation of winter lake ice, which in turn was insulated and prolonged by increased winter snowfall [*Mock et al*. 1998]. Persistence of lake ice into the spring shortens the aquatic growth season and restricts light penetration into the water column

415 during the spring bloom, thereby precluding the growth and development of planktonic
416 communities requiring an ice-free lake for photosynthesis and a turbulent, well-mixed water
417 column. Instead, the mid-late Holocene flora at Heart Lake is dominated by fragilarioid
418 species known to colonise benthic and periphytic habitats under lake ice cover [*Lotter and*
419 *Bigler*, 2000; *Douglas and Smol*, 2010; *Biskaborn et al*. 2016]. These benthic communities
420 would have further benefitted from the absence of competition for nutrients from planktonic
421 diatoms, which do not thrive under ice [*Lepskaya et al*. 2010; *Roberts et al*. 2015]. A
422 reduction in turbulent wind-driven lake mixing at this time may have also been responsible
423 for increased benthic production and a simultaneous expansion of the littoral zone and
424 benthic habitat [*Bradbury*, 1988]. Increased winter precipitation and subsequent spring snow
425 melt would account for the sedimentation increase at 3.8 ka from 0.2 to 0.8 mm/yr [*Krawiec*
426 *and Kaufman*, 2014]. This turbidity would have further reduced light penetration into the
427 benthic zone, thereby promoting fragilarioid taxa which thrive under limited light and
428 generally turbid conditions [*Lotter and Bigler*, 2000; *Douglas and Smol*, 2010].
429 The simultaneous changes in diatom species assemblages and $\delta^{18}O_{diatom}$ values *ca*. 4.4
430 ka reflect numerous factors affecting vertical mixing patterns, availability of resources (e.g.
431 light, nutrients), and thereby the algal production and composition of Heart Lake. These
432 pronounced changes broadly coincided with other paleoenvironmental changes on Adak
433 Island centred *ca*. 4.4 ka. For example the BSi and inferred chlorophyll-*a* record from nearby
434 Andrew Lake also indicates increased aridity after 4.0 ka [*Krawiec and Kaufman*, 2014],
435 while reconstructed plant assemblages show a reduction in *Cyperaceae* after *ca*. 4.5 ka as
436 cooler/drier conditions prevailed over Adak Island [*Heusser*, 1978].
437 Between 950 AD and 1200 AD, higher $\delta^{18}O_{diatom}$ indicates a transition to overall
438 warmer and wetter conditions on Adak (Fig. 5). A decrease in *Empetrum* vegetation across
439 northern Adak also indicates increased moisture [*Heusser*, 1978], while *Krawiec and*
440 *Kaufman* [2014] interpret sustained low BSi and chlorophyll-*a* content from Andrew Lake as

441 the stormiest interval on record. Our $\delta^{18}O_{diatom}$ values exhibit high variability between 950
442 and 1900 AD, implying the local climate was also wetter and more variable since 950 AD.
443 These conditions would account for the continued dominance of fragilarioid taxa over this
444 period with unstable lake conditions [*Smol et al.* 2005; *Rühland et al.* 2008; *Hausmann and*
445 *Pienitz*, 2009]. Additionally, a peak in sedimentation *ca*. 1.0 ka, attributed to increased
446 storminess [*Krawiec and Kaufman*, 2014], rendered conditions unfavourable for planktonic
447 diatom species due to increased sediment suspension and reduced light penetration. Unlike
448 numerous diatom assemblage records across the subarctic and Arctic, in Heart Lake there is
449 no major shift toward those taxa favouring longer growing seasons under warming climatic
450 conditions (e.g. *Cyclotella*) [*Smol et al*. 2005]. Conversely, benthic assemblages show an
451 increase after *ca.* 1860 AD (Fig. 3), reflecting an overall strengthening of Aleutian Low
452 circulation since 1900 AD [*Trenberth and Hurrell*, 1994] and increasingly unstable
453 environmental conditions on Adak Island over the past century. These findings are consistent
454 with observations in North America and Greenland that suggest shifts in *Cyclotella*
455 abundances are more closely related to lake mixing, water clarity and resource availability,
456 rather than direct temperature effects [*Saros and Anderson*, 2015].
457
458 **5.3. Regional paleoenvironmental context**
459 Our $\delta^{18}O_{diatom}$ reconstruction reveals distinct shifts in the prevailing trajectory of storm
460 systems delivering moisture to Adak Island. The primary trends suggest a relatively weak and
461 westerly positioned Aleutian Low during the early-mid Holocene (9.7−4.5 ka), with a
462 strengthening eastward shift after *ca*. 4.5 ka (Fig. 5). Based on 21st century observations,
463 typical climatic responses to a weakened Aleutian Low are: (1) a weakening of Pacific mid-
464 latitude storm tracks; (2) increased meridional flow to the central-western Bering Sea; and (3)
465 reduced winter sea surface heat loss in the central-western Bering Sea and enhanced heat loss
466 from the Okhotsk Sea [*Mock et al*. 1998; *Rodionov et al.* 2007]. Under this synoptic regime

467 the following conditions would be anticipated in regional paleoclimate records: (1) a
468 reduction in winter storms and precipitation in the Gulf of Alaska region; (2) positive
469 precipitation and temperature anomalies in the central-western Aleutian Islands; and (3) SST
470 warming and reduced winter sea ice extent in the central-western Bering Sea and contrary
471 conditions in the Okhotsk Sea.

472 In support of this synoptic-scale picture, vegetation and lake-level reconstructions
473 provide independent evidence for considerably drier winter conditions in eastern Beringia
474 during the early-mid Holocene [*Anderson et al*. 2005; *RS Anderson et al*., 2006; *Zander et al*.
475 2013]. For example, numerous lakes in southern Alaska and the Yukon record lower-than-
476 present water levels during the early Holocene until *ca*. 8 ka [*Kaufman et al*. 2016], reflecting
477 a combination of higher summer temperatures and lower winter precipitation. Furthermore,
478 an inferred decrease in frequency and intensity of winter storms steered into the Gulf of
479 Alaska accounts for marked episodes of glacial retreat at this time [*Solomina et al*. 2015],
480 driven by reduced winter snowfall/accumulation and negative net mass balance.

481 The SST patterns associated with a weakened wintertime Aleutian Low are also
482 evident during the early-mid Holocene. Relatively warm early Holocene SSTs are
483 documented from the western Bering Sea [*Max et al*. 2012], reflecting a persistently negative
484 phase of the PDO during the early-mid Holocene and an increase in Pacific storms tracking
485 into the region [*Rodionov et al*. 2007]. In the Okhotsk Sea, alkenone-derived SST estimates
486 correspond well with Heart Lake $\delta^{18}O_{diatom}$ between ca. 9.6−5.0 ka (Fig. 7), whereby higher
487 $\delta^{18}O_{diatom}$ and an inferred weak Aleutian Low corresponds to lower early-mid Holocene SSTs
488 [*Max et al*. 2012]. This relationship conforms to modern northerly geostrophic wind
489 anomalies during a weakened and westward displaced Aleutian Low that cool and enhance
490 polynya growth in the Okhotsk Sea [*Itaki and Ikahara*, 2004; *Harada et al*. 2014].
491 Specifically, warm (cold) winter SSTs in the Bering Sea (Okhotsk Sea) presently occur when
492 the Aleutian Low is shifted west and the Siberian High dominates over central western

493 Siberia [*Rodionov et al*. 2007]. These anti-correlated trends also manifest in sea-ice anomalies
494 on weekly to monthly time-scales during the 21st century [*Cavalieri and Parkinson*, 1987]
495 and are linked to the east–west migration of the Siberian High and Aleutian Low.
496 We find independent support for the Holocene migration of the Siberian High from
497 the Pechora Lake $\delta^{18}O$ record in northern Kamchatka [*Hammarlund et al*. 2015] (Fig. 7). A
498 north-eastward shift of the Siberian High, concurrent with a strong and eastward shifted
499 Aleutian Low, is linked to periods of increased winter snow contributions to Pechora Lake
500 and overall lower $\delta^{18}O$ values [*Hammarlund et al*. 2015]. The coherency of abrupt and
501 persistent change between the Heart and Pechora Lake $\delta^{18}O$ records between 9.6−3.5 ka
502 provides convincing evidence that the Aleutian Low−Siberian High system prevailed
503 throughout the early-mid Holocene (Fig. 7). Moreover, we propose that the synchronous
504 west-east migration of these systems may have been partially responsible for the non-linear
505 and heterogeneous climatic patterns reconstructed across east and west Beringia at this time
506 [*Brooks et al*. 2015; *Kaufman et al*. 2016].
507 Maximum values of $\delta^{18}O_{diatom}$ in Heart Lake at 7.6 ka broadly coincide with the
508 northern high-latitude (65 °N) summer insolation maxima *ca*. 8.0 ka (Fig. 7) [*Berger and*
509 *Loutre* 1991]. Significantly ($p < 0.001$) higher $\delta^{18}O_{diatom}$ in Heart Lake − relative to both the
510 modern (1900 AD−present) and long-term (9.6 ka−present) mean $\delta^{18}O_{diatom}$ – implies a HTM
511 in the central Aleutian Islands at 7.6 ka characterized by persistently weak Aleutian Low
512 circulation, and coincident with maximum abundances of warm water indicator species [*Smol*
513 *et al*. 2005] (Fig. 3). Similarly, a Holocene SST maximum is evident *ca*. 7.5 ka in both the
514 northwest Pacific [*Minoshima et al*. 2007] and the subarctic North Pacific [*Harada et al*.
515 2014], and from GCMs which indicate maximum SATs and SSTs in the Bering Sea and
516 Aleutian Islands *ca*. 7.0−8.0 ka [*Renssen et al*. 2012]. In southern Kamchatka, the majority of
517 paleoenvironmental records demonstrate a HTM *ca*. 7.0−5.3 ka [*Brooks et al*. 2015],
518 consistent with warm temperatures across eastern Beringia [*Kaufman et al*. 2016]. These

519 results contrast with previous paleoclimate studies from Alaska and the northwest Pacific that
520 identify an earlier HTM at *ca*. 11.3−9.1 ka [*Kaufman et al*. 2004; *Max et al*. 2012]. Such
521 uncertainty in these early Holocene warming patterns is highlighted by *Zhang et al*. [2017]
522 who found large discrepancies between modelled and reconstructed Holocene temperatures
523 across Alaska. Hence, it is difficult to fully constrain the timing of the HTM in the central
524 Aleutian Islands, particularly given that our record does not extend the full Holocene epoch
525 coupled with a paucity of local alternative studies.
526 Simultaneous shifts in diatom flora and $\delta^{18}O_{diatom}$ after the HTM at *ca*. 4.5 ka indicate
527 multiple and inter-related environmental changes that impacted Heart Lake. These
528 pronounced changes coincide with local proxy inferences demonstrating increased aridity
529 under a prevailing northerly circulation pattern [*Heusser*, 1978; *Corbett et al*. 2010; *Krawiec*
530 *and Kaufman*, 2014]. This mid-Holocene perturbation coincides with a return to cooler
531 conditions, increased winter precipitation and extensive glacial advance in Kamchatka
532 [*Nazarova et al*. 2013; *Barr and Solomina*, 2014; *Meyer et al*. 2015]. Widespread cooling is
533 also evident in eastern Beringia during the late Holocene [*Kaufman et al*. 2016], and
534 mountain glaciers across Alaska advanced between *ca*. 4.5 and 3.0 ka [*Solomina et al*. 2015],
535 in phase with those in Kamchatka and demarking onset of the Neoglacial across Beringia
536 [*Savoskul*, 1999; *Barr and Solomina*, 2014]. Though temperature is proposed as the principal
537 control on regional glacier mass balance through the Holocene [*Solomina et al*. 2015], the
538 observed glacial maxima in Alaska are asynchronous with the timing of pronounced cold
539 intervals [*Kaufman et al*. 2016]. Instead, our data suggest the transition to intensified Aleutian
540 Low circulation after 4.5 ka, coincident with declining summer insolation [*Berger and*
541 *Loutre*, 1991], drove widespread Neoglacial advance through the combined effect of
542 increased winter snowfall under a generally cooler regime, yielding a marked regional
543 positive mass balance perturbation. In particular, we note during the past millennium three
544 intervals of lower $\delta^{18}O_{diatom}$ values between 1275−1350 AD, 1400−1550 AD, and 1700−1850

AD coincide with three well-documented episodes of Little Ice Age (LIA) glacier advance on mainland Alaska (Fig. 5 and 7) [*Calkin et al*. 2001; *Solomina et al*. 2015]. Furthermore, the $\delta^{18}O_{diatom}$ minimum at 1805 AD (+24.6 ‰) marks the culmination of regional LIA glacial advance [*Barclay et al*. 2009; *Calkin et al*. 2001; *Wiles et al*. 2004; *Solomina et al*. 2015] (Fig. 5 and 7).

5.4 Coherency of paleoisotope trends

Several paleoisotope records from Alaska have also been interpreted in terms of synoptic-scale changes in atmospheric circulation and inter-comparison with Heart Lake $\delta^{18}O_{diatom}$ yields many commonalities and insights [*Anderson et al*. 2005; *Fisher et al*. 2004; 2008; *Schiff et al*. 2009; *Jones et al*. 2014; *Hammarlund et al*. 2015] (Fig. 7). For instance, a strong inverse relationship *ca*. 9.5−4.0 ka is apparent with millennial scale $\delta^{18}O_{diatom}$ variations at Mica Lake, in Prince William Sound [*Schiff et al*. 2009] (Fig. 7). Lower Mica Lake $\delta^{18}O_{diatom}$ values indicate precipitation delivered by zonal flow under a weak Aleutian Low, whereby precipitating systems are subject to increased rainout as they pass over the Kenai Peninsula and coastal mountain ranges. Conversely, increased meridional flow during a strong Aleutian Low delivers locally sourced moisture from nearby Gulf of Alaska, thereby reducing distillation and isotope depletion in precipitation, thus yielding higher Mica Lake $\delta^{18}O_{diatom}$ values [*Schiff et al*. 2009]. The reciprocal relationship between precipitation-inferred $\delta^{18}O$ values at Heart and Mica Lakes between *ca*. 9.5−4.0 ka conforms to modelling and empirical analyses of spatial patterns of $\delta^{18}O_P$ [*Berkelhammer et al*. 2012; *Bailey et al*. 2015]. The Horse Trail Fen record from the Kenai lowlands is also comparable to Heart Lake from *ca*. 8.0 ka and demonstrates overall higher $\delta^{18}O$ values during the early Holocene and reflecting generally weak Aleutian Low circulation [*Jones et al*. 2014]. The only other full Holocene paleoisotope record from eastern Beringia is from the Mount Logan ice core [*Fisher et al*. 2008], which exhibits strong correspondence with the Jellybean [*Anderson et al*. 2005] and

571 Heart Lake $\delta^{18}O$ records during the early-mid Holocene (Fig. 7).

572 Secondary, but notable departures between paleoisotope records are evident during
573 the late Holocene (Fig. 7), some of which can be reconciled by considering the detailed, non-
574 linear complexity of atmospheric circulation. For instance between *ca.* 3.0−1.0 ka Heart Lake
575 $\delta^{18}O_{diatom}$ does not exhibit marked excursions to the higher $\delta^{18}O$ values documented in Mt.
576 Logan, Jellybean and Pechora Lakes, interpreted as an interval of pronounced weak Aleutian
577 Low circulation [*Anderson et al*. 2005; *Fisher et al*. 2008; *Hammarlund et al*. 2015]. At Heart
578 Lake, this period is characterized by $\delta^{18}O_{diatom}$ values closer to the Holocene mean (Fig. 7).
579 These differences could reflect prevailing atmospheric patterns characterized by a more
580 southerly displaced western centre of low pressure in the northwest Pacific, which typically
581 results in a higher density of storms being steered into the Gulf of Alaska and eastern
582 Kamchatka Peninsula [*Mock et al*. 1998; *Rodionov et al*. 2007]. Under such conditions,
583 precipitation at Mt. Logan, Jellybean and Pechora Lakes would be relatively ^{18}O-enriched
584 [*Berkelhammer et al*. 2012], whereas Heart Lake would fail to exhibit higher $\delta^{18}O_{diatom}$ values
585 since these storm systems would track south of the Aleutian Islands [*Rodionov et al*. 2007].
586

587 **6. Conclusions**

588 The new datasets and analysis presented here extend modern observations across Alaska and
589 Siberia back through the Holocene to bridge a critical gap in the regional network of proxy-
590 climate records [*Sundqvist et al*. 2014; *Brooks et al*. 2015; *Kaufman et al*. 2016]. Although
591 GCMs typically emphasize insolation as the key driver of Holocene temperature change in
592 Alaska [*Renssen et al*. 2009], we demonstrate a more complex relationship and emphasise the
593 role of moisture availability and transport within the land−atmosphere−ocean system.

594 The Aleutian Islands straddle a critical zone of cyclogenesis that influences regional
595 temperature and precipitation patterns, including the heat and moisture flux between the

extratropical Pacific and Arctic; hence, the variable modes of atmospheric circulation we identify have a wide reaching global influence through atmospheric-oceanic teleconnections. Our empirically-derived understanding of the drivers and magnitude of these past changes provide a means to contextualise contemporary climate trends, along with their potential future trajectory and impact, across Alaska and the wider North Pacific. Specifically, we demonstrate that Holocene shifts in Aleutian Low circulation directly impacted the net mass balance of south-central Alaska's glaciers and ice fields through temperature and precipitation variability [*Solomina et al*. 2015]. Given that Alaska is currently experiencing a period of intensified Aleutian Low circulation, which should be favorable for glacier *growth*, the widespread and well documented 21st century retreat of glaciers and ice cover [*Larsen et al*. 2015] would now appear to be unprecedented within the context of long-term Holocene environmental change.

7. Acknowledgements

This research was funded by NSF award EAR 0823522, NERC grants IP/1202/1110 and IP/1460/0514, and a NERC CASE award to H.L.B. (NE/I528350/1). The research was further supported by a Lloyds of London Fulbright Fellowship award to H.L.B. during the preparation of this manuscript. We thank Yarrow Axford, Anne Krawiec, Caleb Schiff, and David Vaillencourt for their field assistance. The US Fish and Wildlife Service, Alaska Maritime Natural Wildlife Refuge and CPS Polar services provided logistical support and access for fieldwork on Adak Island.

8. Data availability

Key datasets for this study are available in Supplementary Table 1. All data produced by this study (*will be*) available online at the World Data Center for Paleoclimatology (WDC Paleo)

620 (https://www.ncdc.noaa.gov/data-access/paleoclimatology-data) and in the NERC National
621 Geoscience Data Centre (NGDC) (http://www.bgs.ac.uk/services/ngdc/).
622
623 **9. References**

624 Anderson, L., Abbot, M.B., Finney, B.P., and Burns, S.J., (2005), Regional atmospheric
625 circulation change in the North Pacific during the Holocene inferred from lacustrine
626 carbonate oxygen isotopes, Yukon Territory, Canada, *Quat. Res*., 64, 21–35, doi:
627 10.1016/j.yqres.2005.03.005.

628 Anderson, R.S., Hallett, D.J., Berg, E., Jass, R.B., Toney, J.L., De Fontaine, C.S., and
629 DeVolder, A., (2006), Holocene development of boreal forests and fire regimes on the Kenai
630 Lowlands of Alaska, *The Holocene*, 16(6), 791−803, doi: 10.1191/0959683606hol966rp.

631 Anderson, L., Berkelhammer, M., Barron, J.A., Steinman, B.A., Finney, B.P., and Abbott,
632 M.B., (2016), Lake oxygen isotopes as recorders of North American Rocky Mountain
633 hydroclimate: Holocene patterns and variability at multi-decadal to millennial timescales,
634 *Glob. Planet. Change*, 137, 131−148, doi: 10.1016/j.gloplacha.2015.12.021.

635 Andrén, E., Klimaschewski, A., Self, A. E., Amour, N. S., Andreev, A. A., Bennett, K. D.,
636 Conley, D.J., Edwards, T.W.D., Solovieva, N., and Hammarlund, D., (2015), Holocene
637 climate and environmental change in north-eastern Kamchatka (Russian Far East), inferred
638 from a multi-proxy study of lake sediments, *Global Planet. Change*, 134, 41–54, doi:
639 10.1016/j.gloplacha.2015.02.013.

640 Baier, J., Lücke, A., Negendank, J.F., Schleser, G.H., and Zolitschka, B., (2004), Diatom and
641 geochemical evidence of mid-to late Holocene climatic changes at Lake Holzmaar, West-
642 Eifel (Germany), *Quat. Int.*, 113(1), 81−96, doi: 10.1016/S1040-6182(03)00081-8.

643 Bailey, H.L., Henderson, A.C.G., Sloane, H.J., Snelling, A., Leng, M.J., and Kaufman, D.S.,

(2014), The effects of species on lacustrine $\delta^{18}O_{diatom}$ and its implications for environmental reconstructions, *J. Quat. Sci.*, 29, 393–400, doi: 10.1002/jqs.2711.

Bailey, H.L., Kaufman, D.S., Henderson, A.C.G., and Leng, M.J., (2015), Synoptic scale controls on the $\delta^{18}O$ in precipitation across Beringia, *Geophys. Res. Lett.*, 42, 4608−4616, doi: 10.1002/2015GL063983.

Barclay, D.J., Wiles, G.C., and Calkin, P.E., (2009), Holocene glacier fluctuations in Alaska, *Quat. Sci. Rev.*, 28, 2034−2048, doi: 10.1016/j.quascirev.2009.01.016.

Barker, P.A., Street-Perrott, F.A., Leng, M.J., Greenwood, P.B., Swain, D.L., Perrott, R.A., Telford, J., and Ficken, K.J., (2001) A 14 ka oxygen isotope record from diatom silica in two alpine tarns on Mt. Kenya, *Science*, 292, 2307−2310, doi: 10.1126/science.1059612.

Barr, I.D., and Solomina, O., (2014), Pleistocene and Holocene glacier fluctuations upon the Kamchatka Peninsula, *Glob. Planet Change*, 113, 110-120, doi: 10.1016/j.gloplacha.2013.08.005.

Berger, A., and Loutre, M.F., (1991), Insolation values for the climate of the last 10 million years, *Quat. Sci. Rev.*, 10, 297−317, doi:10.1016/0277-3791(91)90033-Q.

Berkelhammer, M., Stott, L., Yoshimura, K., Johnson, K., and Sinha, A., (2012), Synoptic and mesoscale controls on the isotopic composition of precipitation in the western United States, *Climate Dynamics*, 38 (3-4), 433−454, doi: 10.1007/s00382-011-1262-3.

Biskaborn, B.K., Subetto, D.A., Savelieva, L.A., Vakhrameeva, P.S., Hansche, A., Herzschuh, U., Klemm, J., Heinecke, L., Pestryakova, L.A., Meyer, H., and Kuhn, G., (2016), Late Quaternary vegetation and lake system dynamics in north-eastern Siberia: Implications for seasonal climate variability, *Quat. Sci. Rev.*, 147, 406−421, doi: 10.1016/j.quascirev.2015.08.014.

667 Black, R.F., (1976), Late Quaternary glacial events, Aleutian Islands, Alaska. In:
668 Easterbrook, D.D., Sibrava, V. (Eds.), Quaternary Glaciations in the Northern Hemisphere.
669 IUGSUNESCO International Geological Correlations Program, Project 73-1-24. International
670 Union of Quaternary Research, Bellingham, pp. 285–301.

671 Bradbury, P., Cumming, B., and Laird, K., (2002), A 1500-year record of climatic and
672 environmental change in Elk Lake, Minnesota III: measures of past primary productivity, *J.*
673 *Paleolimnol.*, 27(3), 321−340, doi: 10.1023/A:1016035313101.

674 Bradley, C.C., (1948), Geologic notes on Adak Island and the Aleutian chain, Alaska, *Am. J.*
675 *Sci.*, 246(4), 214-240, doi: 10.2475/ajs.246.4.214.

676 Brooks, S.J., Diekmannb, B., Jones, V.J., and Hammarlund, D., (2015), Holocene
677 environmental change in Kamchatka: A synopsis, *Glob. Planet Change*, 134, 166−174, doi:
678 10.1016/j.gloplacha.2015.09.004.

679 Calkin, P.E., Wiles, G.C., and Barclay, D. J., (2001), Holocene coastal glaciation of Alaska,
680 *Quat. Sci. Rev.*, 20, 449−461, doi: 10.1016/S0277-3791(00)00105-0.

681 Camburn, K.E., and Charles, D.F., (2000), *Diatoms of Low-alkalinity Lakes in the*
682 *Northeastern United States,* ANSP Special Publication 18. Academy of Natural Sciences of
683 Philadelphia, Philadelphia.

684 Cavalieri, D.J., and Parkinson, C.L., (1987), On the relationship between atmospheric
685 circulation and the fluctuations in the sea ice extents of the Bering and Okhotsk Seas, *J.*
686 *Geophys. Res.*, 92, 7141–7162, doi: 10.1029/JC092iC07p07141.

687 Chapligin, B., Narancic, B., Meyer, H., and Pienitz, R., (2016), Paleo-environmental
688 gateways in the eastern Canadian arctic–Recent isotope hydrology and diatom oxygen

689 isotopes from Nettilling Lake, Baffin Island, Canada, *Quat. Sci. Rev.*, 147, 379–390, doi:
690 10.1016/j.quascirev.2016.03.028.

691 Clayton, R.N., and Mayeda, T.K., (1963), The use of bromine pentafluoride in the extraction
692 of oxygen from oxide and silicates for isotopic analysis, *Geochim. Cosmochim. Acta*, 27, 43–
693 52, doi: 10.1016/0016-7037(63)90071-1.

694 Clegg, B.F., and Hu, F.S., (2010), An oxygen-isotope record of Holocene climate change in
695 south-central Brooks Range, Alaska, *Quat. Sci. Rev.*, 29, 928–939, doi:
696 10.1016/j.quascirev.2009.12.009.

697 Coats, R.R., (1956), *Reconnaissance geology of some western Aleutian Islands, Alaska,* US
698 Geological Survey Bulletin 1028-E, Government Printing Office.

699 Corbett, D., West, D., and Lefevre, C., (2010), *The People at the End of the World: The*
700 *Western Aleutian Project and the Archeology of Shemya Island,* Alaska Anthropological
701 Association Monograph Series VIII.

702 Devlin, J.E., and Finkelstein, S.A., (2011), Local physiographic controls on the responses of
703 Arctic lakes to climate warming in Sirmilik National Park, Nunavut, Canada, *J. Paleolimnol.*,
704 45(1), 23–39, doi: 10.1007/s10933-010-9477-6.

705 Douglas, M.S.V., and Smol, J.P., (2010*), Freshwater diatoms as indicators of environmental*
706 *change in the High Arctic*, In: Smol, J.P., Stoermer, E.F. (Eds.), The Diatoms: Application for
707 the Environmental and Earth Sciences. Cambridge University Press, Cambridge, pp.
708 249–266.

709 Fisher, D.A., Wake, C., Kreutz, K., Yalcin, K., Steig, E., Mayewski, P., Anderson, L., Zheng,
710 J., Rupper, S., Zdanowicz, C., Demuth, M., Waszkiewicz, M., Dahl-Jensen, D., Goto-Azuma,
711 K., Bourgeois, J.B., Koerner, R.M., Sekerka, J., Osterberg, E., Abbott, M.B., Finney, B.P.,

712 and Burn, S.J., (2004), Stable isotope records from Mount Logan, Eclipse ice cores and
713 nearby Jellybean Lake. Water cycle of the North Pacific over 2000 years and over five
714 vertical kilometres: Sudden shifts and tropical connections, *Geogr. Phys. Quat*., 58 (2–3),
715 337–352, doi: 10.7202/013147ar.

716 Fisher, D., Osterberg, E., Dyke, A., Dahl-Jensen, D., Demuth, M., Zdanowicz, C., Bourgeois,
717 J., Koerner, R.M., Mayewski, P., Wake, C., Kreutz, K., Steig, E., Zheng, J., Yalcin, K., Goto-
718 Azuma, K., Luckman B., and Rupper, S., (2008), The Mt Logan Holocene-late Wisconsinan
719 isotope record: tropical Pacific--Yukon connections, *The Holocene*, 18, 667−677, doi:
720 10.1177/0959683608092236.

721 Fraser, G.D., and Snyder, G.L., (1959), *Geology of southern Adak Island and Kagalska*
722 *Island, Alaska*, US Geological Survey Bulletin 1028, pp. 371−408.

723 Gibson, C.E., Anderson, N.J., and Haworth, E.Y., (2003), Aulacoseira subarctica: taxonomy,
724 physiology, ecology and palaeoecology, *Eur. J. Phycol*., 38, 83−101, doi:
725 10.1080/0967026031000094102.

726 Grimm, E.C., (1987), Coniss - a Fortran-77 program for stratigraphically constrained cluster-
727 analysis by the method of incremental sum of squares. *Comput. Geosci*., 13, 13−35.

728 Grimm, E.C., (2015) TILIA software. Version *2.0.41*. https://www.tiliait.com/download/

729 Hammarlund, D., Klimaschewski, A., St. Amour, N.A., Andrén, E., Self, A.E., Solovieva, N.,
730 Andreev, A.A., Barnekowa, L., and Edwards, T.W.D, (2015), Late Holocene expansion of
731 Siberian dwarf pine (*Pinus pumila*) in Kamchatka in response to increased snow cover as
732 inferred from lacustrine oxygen-isotope records, *Glob. Planet. Change*, 134, 91−100, doi:
733 10.1016/j.gloplacha.2015.04.004.

Harada, N., Katsuki, K., Nakagawa, M., Matsumoto, A., Seki, O., Addison, J.A., Finney, B.P., and Sato, M., (2014), Holocene sea surface temperature and sea ice extent in the Okhotsk and Bering Seas, *Prog. Oceanogr.*, 126, 242−253, doi: 10.1016/j.pocean.2014.04.017.

Hausmann, S., and Pienitz, R., (2009), Seasonal water chemistry and diatom changes in six boreal lakes of the Laurentian Mountains (Québec, Canada): impacts of climate and timber harvesting, *Hydrobiologia*, 635(1), 1−14, doi: 10.1007/s10750-009-9855-0.

Heusser, C.J., (1978), Post-glacial vegetation on Adak Island, Aleutian Islands, Alaska. *Bull. Torrey Bot. Club*., 105, 18–23, doi: 10.2307/2484259.

Hoff, U., Biskaborn, B.K., Dirksen, V.G., Dirksen, O., Kuhn, G., Meyer, H., Nazarova, L., Roth, A., and Diekmann, B., (2015), Holocene environment of Central Kamchatka, Russia: Implications from a multi-proxy record of Two-Yurts Lake, *Glob. Planet. Change*, 134, 101−117, doi: 10.1016/j.gloplacha.2015.07.011.

Horn, H., Paul, L., Horn, W., and Petzoldt, T., (2011), Long-term trends in the diatom composition of the spring bloom of a German reservoir: is *Aulacoseira subarctica* favoured by warm winters? *Fresh. Biol.*, 56(12), 2483−2499, doi: 10.1111/j.1365-2427.2011.02674.x.

IAEA/WMO, (2017), *Global Network of Isotopes in Precipitation,* The GNIP Database. Accessible at: http://www.iaea.org/water.

Interlandi, S.J., Kilham, S.S., and Theriot, E.C., (1999), Responses of phytoplankton to varied resource availability in large lakes of the Greater Yellowstone Ecosystem, *Limnol. Oceanogr*, 44(3), 668−682, doi: 10.4319/lo.1999.44.3.0668.

Itaki, T., and Ikehara, K., (2004), Middle to late Holocene changes of the Okhotsk Sea Intermediate Water and their relation to atmospheric circulation, *Geophys. Res. Lett.*, 31, L24309, doi: 10.1029/2004GL021384.

Jones, V.J., Leng, M.J., Solovieva, N., Sloane, H.J. and Tarasov, P., (2004) Holocene climate of the Kola Peninsula; evidence from the oxygen isotope record of diatom silica, *Quat. Sci. Rev.*, 23(7−8), 833−839, doi: 10.1016/j.quascirev.2003.06.014.

Jones, M. C., Wooller, M., and Peteet, D.M., (2014), A deglacial and Holocene record of climate variability in south-central Alaska from stable oxygen isotopes and plant macrofossils in peat, *Quat. Sci. Rev.*, 87, 1–11, doi: 10.1016/j.quascirev.2013.12.025.

Juggins, S., (2014), C2 Data Analysis. Version 1.7.6. University of Newcastle, Newcastle.

Kalnay, E. *et al*. (1996), The NCEP/NCAR 40-Year Reanalysis Project. *Bull. Am. Meteorol. Soc*., 77, 437−471.

Kaufman, D.S., Ager, T.A., Anderson, N.J., Anderson, P.M., Andrews, J.T., Bartelein, P.J., Burbaker, L.B., Coats, L.L., Cwynar, L.C., Duval, M.L., Dyke, A.S., Edwards, M.E., Eiser, W.R., Gajewski, K., Geisodottir, A., Hu, F.S., Jennings, A.E., Kaplan, M.R., Kewin, M.W., Lozhkin, A.V., MacDonald, G.M., Miller, G.H., Mock, C.J., Oswald, W.W., Otto-Blisner, B.L., Porinchu, D.F., Rühland, K., Smol, J.P., Steig, E.J., and Wolfe, B.B., (2004), Holocene thermal maximum in the western Arctic (0-180° W), *Quat. Sci. Rev*., 23, 529−560, doi: 10.1016/j.quascirev.2003.09.007.

Kaufman, D.S., Axford, Y.L., Henderson, A.C.G., McKay, N.P., Oswald, W.W., Saenger, C., Anderson, R.S., Bailey, H.L., Clegg, B., Gajewski, K., Sheng Hu, F., Jones, M.C., Massa, C. Routson, C.C., Werner, A., Wooller, M.J., and Yu, Z., (2016), Holocene climate changes in eastern Beringia (NW North America) — A systematic review of multi-proxy evidence, *Quat. Sci. Rev.*, 147, 312−339, doi: 10.1016/j.quascirev.2015.10.021.

779 Krammer, K., and Lange-Bertalot, H., (1986−1991), *Bacillariophyceae Band 2/2*. Gustav
780 Fischer Verlag, Stuttgart, pp.1−4.

781 Krawiec, A.C.L, and Kaufman, D.S., (2014), Holocene storminess inferred from sediments of
782 two lakes on Adak Island, Alaska, *Quaternary Res*., 82, 73−84, doi:
783 10.1016/j.yqres.2014.02.007.

784 Krawiec, A.C.L, Kaufman, D.S., and Vaillencourt, D.A., (2013), Age models and
785 tephrostratigraphy from two lakes on Adak Island, Alaska. *Quat. Geochronol*., 18, 41−53,
786 doi: 10.1016/j.quageo.2013.07.002.

787 Labeyrie, L.D., (1974), New approach to surface seawater palaeotemperatures using $^{18}O/^{16}O$
788 ratios in silica of diatom frustules, *Nature*, 248, 40–42, doi: 10.1038/248040a0.

789 Lachniet, M.S., Lawson, D.E., Stephen, H., Sloat, A.R., and Patterson, W.P., (2016),
790 Isoscapes of $\delta^{18}O$ and $\delta^{2}H$ reveal climatic forcings on Alaska and Yukon precipitation, *Water*
791 *Resour. Res*., 52(8), 6575−6586, doi: 10.1002/2016WR019436.

792 Lamb., A.L., Brewer, T.S., Leng, M.J., Sloane, H.J., and Lamb, H.F., (2007), A geochemical
793 method for removing the effect of tephra on lake diatom oxygen isotope records, *J.*
794 *Paleolimnol*., 37, 499−516, doi: 10.1007/s10933-006-9034-5.

795 Larsen, C.F., Burgess, E., Arendt, A.A., O'neel, S., Johnson, A.J. and Kienholz, C., (2015),
796 Surface melt dominates Alaska glacier mass balance, *Geophys. Res. Lett.*, 42(14),
797 5902−5908, doi: 10.1002/2015GL064349. .

798 Leclerc, A.J., and Labeyrie, L., (1987), Temperature dependence of the oxygen isotopic
799 fractionation between diatom silica and water, *Earth Planet. Sci. Lett.*, 84(1), 69−74, doi:
800 10.1016/0012-821X(87)90177-4.

Leng, M.J., and Barker, P.A., (2006), A review of the oxygen isotope composition of lacustrine diatom silica for paleoclimate reconstruction, *Earth Sci. Rev.*, 75, 5–27, doi: 10.1016/j.earscirev.2005.10.001.

Leng, M.J., and Sloane, H.J., (2008), Combined oxygen and silicon isotope analysis of biogenic silica, *J. Quat. Sci*., 23, 313–319, doi: 10.1002/jqs.1177.

Leng, M., Barker, P., Greenwood, P., Roberts, N., and Reed, J., (2001), Oxygen isotope analysis of diatom silica and authigenic calcite from Lake Pinarbasi, Turkey, *J. Paleolimnol.*, 25(3), 343−349, doi: 10.1023/A:1011169832093.

Lepskaya, E.V., Jewson, D.H., and Usoltseva, M.V., (2010), *Aulacoseira subarctica* in Kurilskoye Lake, Kamchatka: a deep, oligotrophic lake and important Pacific salmon nursery, *Diatom Research*, 25(2), 323−335, doi: 10.1080/0269249X.2010.9705853.

Lotter, A.F., and Bigler, C., (2000), Do diatoms in the Swiss Alps reflect the length of ice-cover? *Aquatic Sciences*, 62(2), 125−141, doi: 10.1007/s000270050002.

Lotter, A.F., Pienitz, R., and Schmidt, R., (2010), *Diatoms as indicators of environmental change in subarctic and alpine regions*, In: Smol, J.P., Stoermer, E.F. (Eds.), The Diatoms: Application for the Environmental and Earth Sciences. Cambridge University Press, Cambridge.

Mackay, A.W., Swann, G.E.A., Brewer, T.S., Leng, M.J., Morley, D.W., Piotrowska, N., Rioual, P., and White, D., (2011), A reassessment of late glacial—Holocene diatom oxygen isotope record from Lake Baikal using a geochemical mass-balance approach, *J. Quat. Sci.* 26, 627–634, doi: 10.1002/jqs.1484.

822 Mantua, N.J., Hare, S.R., Zhang, Y., Wallace, J.M., and Francis, R.C., (1997), A Pacific
823 interdecadal climate oscillation with impacts on salmon production, *Bull. Am. Meteorol. Soc*.,
824 78, 1069−1079, doi: 10.1175/1520-0477(1997)078<1069:APICOW>2.0.CO;2.

825 Marcott, S.A., Shakun, J.D., Clark, P.U., and Mix, A.C., (2013), A reconstruction of regional
826 and global temperature for the past 11 300 years, *Science*, 339, 1198−1201, doi:
827 10.1126/science.1228026.

828 Max, L., Riethdorf, J-R., Tiedemann R., Smirnova, M., Lembke-Jene, L., Fahl, K., Nürnberg,
829 D., Matul, A., and Mollenhauer, G., (2012), Sea surface temperature variability and sea-ice
830 extent in the subarctic northwest Pacific during the past 15,000 years, *Paleoceanography*, 27,
831 PA3213, doi:10.1029/2012PA002292.

832 Mayewski, P.A., Rohling, E.E., Stager, J.C., Karlén, K.A., Maasch,W., Meeker, L.D.,
833 Meyerson, E.A., Gasse, F., van Kreveld, S., Holmgren, K., Lee-Thorp, J., Rosqvist, G., Rack,
834 F., Staubwasser, M., Schneider, R.R., and Steiger, E.J., (2004), Holocene climate variability,
835 *Qual. Res*., 62, 243–255, doi: 10.1016/j.yqres.2004.07.001.

836 Meyer, H., Chapligin, B., Hoff, U., Nazarova, L., and Diekmann, B., (2015), Oxygen isotope
837 composition of diatoms as Late Holocene climate proxy at Two-Yurts-Lake, Central
838 Kamchatka, Russia. *Glob. Planet. Chang.*, 134, 118–128, doi:
839 10.1016/j.gloplacha.2014.04.008.

840 Minoshima, K., Kawahata, H., and Ikehara, K., (2007), Changes in biological production in
841 the mixed water region (MWR) of the northwestern North Pacific during the last 27 kyr,
842 *Palaeogeogr. Palaeoclimatol. Palaeoecol*., 254, 430−447, doi:10.1016/j.palaeo.2007.06.022.

843 Mock, C. J., Bartlein, P. J., and Anderson, P. M., (1998), Atmospheric circulation patterns
844 and spatial climatic variations in Beringa, *Int. J. Climatol*., 10, 1085–1104,
845 doi:10.1002/(SICI)1097-0088(199808)18:10<1085::AID-JOC305>3.0.CO;2-K.

Morley, D.W., Leng, M.J., Mackay, A.W., Sloane, H.J., Rioual, P. and Battarbee, R.W., (2004), Cleaning of lake sediment samples for diatom oxygen isotope analysis, *J. Paleolimnol.*, 31(3), 391−401, doi: 10.1023/B:JOPL.0000021854.70714.6b.

Nazarova, L., de Hoog, V., Hoff, U., Dirksen, O., and Diekmann, B., (2013), Late Holocene climate and environmental changes in Kamchatka inferred from the subfossil chironomid record, *Quat. Sci. Rev*., 67, 81–92, doi: 10.1016/j.quascirev.2013.01.018.

NOAA, (2017), National Oceanic and Atmospheric Administration. National Climatic Data Centre. https://www.ncdc.noaa.gov/land-based-station-data.

Rehfeld, K., Münch, T., Ho, S.L., and Laepple, T., (2018), Global patterns of declining temperature variability from the Last Glacial Maximum to the Holocene, *Nature*, 554 (7692), 356−359, doi:10.1038/nature25454.

Renssen, H., Seppä, H, Heiri, O., Goosse, H., and Fichefet, T., (2009), The spatial and temporal complexity of the Holocene thermal maximum, *Nat. Geosci*., 2, 411–414, doi: 10.1038/ngeo513.

Renssen, H., Seppä, H., Crosta, X., Goosse, H., and Roche, D.M., (2012), Global characterization of the Holocene Thermal Maximum, *Quat. Sci. Rev*., 48, 7−19, doi: 10.1016/j.quascirev.2012.05.022.

Rioual, P., Andrieu-Ponel, V., Rietti-Shati, M., Battarbee, R.W., de Beaulieu, J.L., Cheddadi, R., Reille, M., Svobodova, H., and Shemesh, A., (2001), High-resolution record of climate stability in France during the last interglacial period, *Nature*, 413(6853), 293−296, doi: 10.1038/35095037.

Rioual, P., Andrieu-Ponel, V., de Beaulieu, J.L., Reille, M., Svobodova, H., and Battarbee, R.W., (2007), Diatom responses to limnological and climatic changes at Ribains Maar

(French Massif Central) during the Eemian and Early Würm, *Quat. Sci. Rev.*, 26(11), 1557−1609, doi: 10.1016/j.quascirev.2007.03.009.

Roberts, S., Jones, V.J., Allen, J.R., and Huntley, B., (2015), Diatom response to mid-Holocene climate in three small Arctic lakes in northernmost Finnmark, *The Holocene*, 25(6), 911−920, doi: 10.1177/0959683615572853.

Rodionov, S. N., Bond, N.A., and Overland, J.E., (2007), The Aleutian Low, storm tracks, and winter climate variability in the Bering Sea, *Deep Sea Res.II.*, 54, 2560–2577, doi: 10.1016/j.dsr2.2007.08.002.

Rosqvist, G., Jonsson, C., Yam, R., Karlén, W., and Shemesh, A., (2004), Diatom oxygen isotopes in pro-glacial lake sediments from northern Sweden: a 5000 year record of atmospheric circulation, *Quat. Sci. Rev.*, 23(7), 851−859, doi: 10.1016/j.quascirev.2003.06.009.

Rühland, K., Priesnitz, A., and Smol, J.P., (2003), Paleolimnological evidence from diatoms for recent environmental changes in 50 lakes across Canadian Arctic treeline, *Arct. Antarct. Alp. Res.*, 35(1), 110−123, doi: 10.1657/1523-0430(2003)035[0110:PEFDFR]2.0.CO;2.

Rühland, K., Paterson, A.M., and Smol, J.P., (2008), Hemispheric-scale patterns of climate-related shifts in planktonic diatoms from North American and European lakes, *Glob. Change Biol.*, 14(11), 2740−2754, doi: 10.1111/j.1365-2486.2008.01670.x.

Saros, J.E. and Anderson, N.J., 2015. The ecology of the planktonic diatom Cyclotella and its implications for global environmental change studies, *Biol. Rev.*, 90(2), 522−541, doi: 10.1111/brv.12120.

Savoskul, O.S., (1999), Holocene glacier advances in the headwaters of Sredniaya Avacha, Kamchatka, Russia, *Qual. Res.*, 52, 14–26, doi: 10.1006/qres.1999.2051.

892 Schiff, C.J., Kaufman, D.S., Wolfe, A.P., Dodd, J., and Sharp, Z., (2009), Late Holocene
893 storm-trajectory changes inferred from the oxygen isotope composition of lake diatoms, south
894 Alaska, *J. Paleolimnol.*, 41, 189–208, doi: 10.1007/s10933-008-9261-z.

895 Smol, J. P., Wolfe, A. P., Birks, H. J. B., Douglas, M. S., Jones, V. J., Korhola, A., Pienitz,
896 R., Rühland, K., Sorvari, S., Antoniades, D., and Brooks, S. J., (2005), Climate-driven regime
897 shifts in the biological communities of arctic lakes., *PNAS*, 102(12), 4397−4402, doi:
898 10.1073/pnas.0500245102.

899 Solomina, O.N., Bradley, R.S., Hodgson, D.A., Ivy-Ochs, S., Jomelli, V., Macintosh, A.N.,
900 Nesje, A., Owen, L.A.,Wanner, H., Wiles, G.C., and Young, N.E., (2015), Holocene glacier
901 fluctuations, *Quat. Sci. Rev.*, 111, 9−34, doi: 10.1016/j.quascirev.2014.11.018.

902 Solovieva, N., Klimaschewski, A., Self, A. E., Jones, V. J., Andrén, E., Andreev, A. A.,
903 Hammarlund, D., Lepskaya, E.V., and Nazarova, L., (2015), The Holocene environmental
904 history of a small coastal lake on the north-eastern Kamchatka Peninsula, *Glob. Planet.*
905 *Change*, 134, 55–66, doi: 10.1016/j.gloplacha.2015.06.010.

906 Spaulding, S.A., Lubinski, D.J. and Potapova, M., (2017), Diatoms of the United States.
907 http://westerndiatoms.colorado.edu

908 Streletskiy, D.A., Tananaev, N.I., Opel, T., Shiklomanov, N.I., Nyland, K.E., Streletskaya,
909 I.D. and Shiklomanov, A.I., (2015), Permafrost hydrology in changing climatic conditions:
910 seasonal variability of stable isotope composition in rivers in discontinuous permafrost.
911 *Environ. Res. Lett.*, 10 (9), p.095003, doi: 10.1088/1748-9326/10/9/095003.

912 Sundqvist, H.S., Kaufman, D.S., McKay, N.P., Balascio, N.L., Briner, J.P., Cwynar, L.C.,
913 Sejrup, H.P., Seppä, H., Subetto, D.A., Andrews, J.T. and Axford, Y., (2014), Arctic
914 Holocene proxy climate database–new approaches to assessing geochronological accuracy

915 and encoding climate variables *Clim. Past*, 10(4), 1605−1631, doi: 10.5194/cp-10-1605-
916 2014.

917 Swann, G.E.A., and Patwardhan, S.V., (2011), Application of Fourier Transform Infrared
918 Spectroscopy (FTIR) for assessing biogenic silica sample purity in geochemical analyses and
919 palaeoenvironmental research, *Clim*. *Past*, 7, 65–74, doi: 10.5194/cp-7-65-2011.

920 TDX (2013), TDX Power - Adak Reconnaissance Study. *Hatch*.
921 http://akenergyinventory.org/hyd/SSH-2013-0004.pdf

922 ter Braak, C.J.F., and Prentice, I.C., (1988), A theory of gradient analysis, *Adv*. *Ecol*. *Res*.,
923 18, 271–317, doi: 10.1016/S0065-2504(03)34003-6.

924 Trenberth, K.E., and Hurrell, J.W., (1994), Decadal atmosphere-ocean variations in the
925 Pacific, *Clim. Dyn.*, 9, 303–319, doi: 10.1007/BF00204745.

926 *USGS*, (2017), USGS *Landsat* 8 Images. Available at: https://landsat.gsfc.nasa.gov/

927 Vachula, R.S., Chipman, M.L., and Hu, F.S., (2017), Holocene climatic change in the
928 Alaskan Arctic as inferred from oxygen-isoope and lake-sediment analyses at Wahoo Lake,
929 *The Holocene*, 27 (4), 1−14, doi: https://doi.org/10.1177/0959683617702230.

930 Walker, M., Berhelhammer, M., Bj€orck, S., Cwynar, L.C., Fisher, D.A., Long, A.J., Lowe,
931 J.J., Newnham, R.M., Rasmussen, S.O., and Weis, H., (2012), Formal subdivision of the
932 Holocene Series/Epoch: a discussion Paper by a Working Group of INTIMATE (Integration
933 of ice-core, marine and terrestrial records) and the Subcommission on Quaternary
934 Stratigraphy (International Commission on Stratigraphy), *J. Quat. Sci*., 27, 649−659, doi:
935 10.1002/jqs.2565.

936 Wang, L., Lu, H., Liu, J., Gu, Z., Mingram, J., Chu, G., Li, J., Rioual, P., Negendank, J.F.,
937 Han, J., and Liu, T., (2008), Diatom-based inference of variations in the strength of Asian

938 winter monsoon winds between 17,500 and 6000 calendar years BP, *J. Geophys. Res. Atmos.*,
939 113, D2101, doi: 10.1029/2008JD010145.

940 Welker, J.M., (2000), Isotopic ($\delta^{18}O$) characteristics of weekly precipitation collected
941 across the USA: an initial analysis with application to water source studies, *Hydrol.*
942 *Process.*, 14(8), 1449−1464, doi: 10.1002/1099-1085(20000615)14:8<1449::AID-
943 HYP993>3.0.CO;2-7.

944 Wiles, G., D'Arrigo, R., Villalba, R., Calkin, P., and Barclay, D.J., (2004), Century-scale
945 solar variability and Alaskan temperature change over the past millennium, *Geophys.*
946 *Res. Lett.* 31, L15203, doi: 10.1029/2004GL020050.

947 Zander, P.D., Kaufman, D.S., Kuehn, S.C.,Wallace, K.L., and Anderson, R.S., (2013), Early
948 and late Holocene glacial fluctuations and tephrostratigraphy, Cabin Lake, Alaska, *J. Quat.*
949 *Sci*., 28, 761−771, doi: 10.1002/jqs.2671

950 Zhang, Y., Renssen, H., Seppä, H., and Valdes, P.J., (2017), Holocene temperature
951 evolution in the Northern Hemisphere high latitudes–Model-data comparisons, *Quat. Sci.*
952 *Rev.*, 173, 101−113, doi: 10.1016/j.quascirev.2017.07.018.

953 **Author contributions**

954 D.S.K was PI, led the fieldwork and retrieved the sediment cores. D.S.K., H.L.B, H.J.S.,
955 A.C.G.H. and M.J.L developed the study concept. H.L.B conducted the research, sample
956 preparation, SEM, diatom and statistical analyses, interpreted the results, produced the
957 figures, and wrote the original manuscript. D.S.K. and A.L.H. critically revised the original
958 manuscript, and together with H.M. and J.M.W. provided technical advice and comments.
959 H.J.S performed the FTIR and diatom isotope measurements. M.J.L. supervised the diatom
960 isotope measurements and undertook the isotope corrections. H.J.S., A.C.G.H., M.J.L., H.M.
961 and J.M.W provided minor editorial revisions. All authors approved the final manuscript.

962 The authors declare no competing financial interests.

963

964 **Figure captions**

965

966 **FIG1.JPG** [Image size: 1.5 page width]

967 Figure 1. Location of (a) Adak Island in the central Aleutian Islands, (b) Heart Lake and
968 Andrew Lake, (c) oblique north west view of Heart Lake with the inflow channel visible in
969 the foreground [credit: Yarrow Axford], and (d) monthly mean precipitation (blue bars) and
970 surface air temperature at Adak airport (1949−2016), whereby solid lines depict mean
971 (black), minimum (blue) and maximum (red) temperatures [*NOAA*, 2017]. Numbered circles
972 in 1a indicate key sites referred to in text: (1) LV29-114-3 [*Max et al*. 2012], (2) Pechora
973 Lake [*Hammarlund et al*. 2015], (3) SO201-12-77KL [*Max et al.* 2012], (4) Horse Trail Fen
974 [*Jones et al*. 2014], (5) Mica Lake [*Schiff et al*. 2009], (6) Mount Logan [*Fisher et al*. 2008],
975 and (7) Jellybean Lake [*Anderson et al*. 2005]

976

977 **FIG2.JPG** [Image size: Column width]

978 Figure 2. Mean winter (December−February) sea level pressure associated with the six most
979 positive (a) and negative (b) North Pacific Index (NPI) values between 1950 and 2017
980 [*Trenberth and Hurrell*, 1994]. A negative (positive) NPI is a strong (weak) Aleutian Low.
981 Arrows highlight the direction of the primary storm tracks delivering precipitation to our site
982 on Adak Island (yellow star) [*Bailey et al.* 2015]. SLP data obtained from NCEP/NCAR V1
983 reanalysis [*Kalnay et al*. 1996]. Numbered yellow circles in (a) indicate locations of the (1)
984 LV29-114-3 [*Max et al.* 2012], (2) Pechora Lake [*Hammarlund et al*. 2015], (3) SO201-12-
985 77KL [*Max et al*.2012], (4) Horse Trail Fen [*Jones et al.* 2014], (5) Mica Lake [*Schiff et al*.
986 2009], (6) Mount Logan [*Fisher et al*. 2008], and (7) Jellybean Lake [*Anderson et al*. 2005]
987 climate records discussed in text

FIG3.PDF [Image size: Full page width]

Figure 3. Heart Lake diatom stratigraphy and Principal Components Analysis (PCA) scores of the 11 dominant diatom species (>5 % abundance), grouped by habitat preference. Diatom zone demarcation (dashed lines 1−4) is guided by the CONISS cluster analysis. Variables are plotted on a linear timescale (ka BP) and the depth scale refers to depth below lake floor

FIG4.PDF [Image size: Column width]

Figure 4. Loadings of the 11 dominant diatom taxa from Heart Lake and their corresponding PCA scores. Sample scores (circles) are coloured according to their down core diatom assemblage Zone (1−4). Dashed coloured ellipses group diatom species by their habitat preference

FIG5.PDF **[**Image size: Full page width]

Figure 5. Time series of Heart Lake $\delta^{18}O_{diatom}$ during (a) the past millennium and (b) the Holocene. Horizontal dashed grey lines indicate the Holocene and the 21st century mean $\delta^{18}O_{diatom}$ value. Orange diamonds and white triangles indicate previously published radiocarbon ages and tephra beds, respectively [*Krawiec et al*. 2013]. Vertical blue bars correspond to three intervals of Little Ice Age glacier advance in mainland Alaska [*Solomina et al*. 2015]

FIG6.PDF [Image size: Column width]

Figure 6. Heart Lake bottom water $\delta^{18}O$ (2009 and 2010) on the local meteoric water line (LMWL) and the global meteoric water line (GMWL). LMWL data are derived from Adak monthly composite precipitation samples collected by the Global Network of Isotopes in Precipitation (GNIP) [*IAEA/WMO*, 2017]

FIG7.PDF [Image size: Column width]

Figure 7. Holocene time series of (a) summer (JJA) insolation at 65°N [*Berger and Loutre*, 1991], (b) alkenone SSTs from LV29-114-3 in the Okhotsk Sea [*Max et al*. 2012], (c) Pechora Lake $\delta^{18}O$ [*Hammarlund et al*. 2015], (d) Heart Lake $\delta^{18}O_{diatom}$ (this record), (e) intervals of expanded mountain glaciers in eastern Beringia [*Solomina et al*. 2015], (f) Mica Lake $\delta^{18}O$ [*Schiff et al*. 2009], (g) Mount Logan ice $\delta^{18}O$ [*Fisher et al*. 2008], (h) Horse Trail Fen $\delta^{18}O$ [*Jones et al*. 2014], and (i) Jellybean Lake $\delta^{18}O$ [*Anderson et al*. 2005]. Black lines in (g) and (i) represent 40-yr smoothed intervals. Vertical red shading indicates the eastern Beringia mid-Holocene Thermal Maximum [*Kaufman et al*. 2016], blue shading indicates the Little Ice Age (LIA) [*Solomina et al*. 2015]

Figures

FIG1

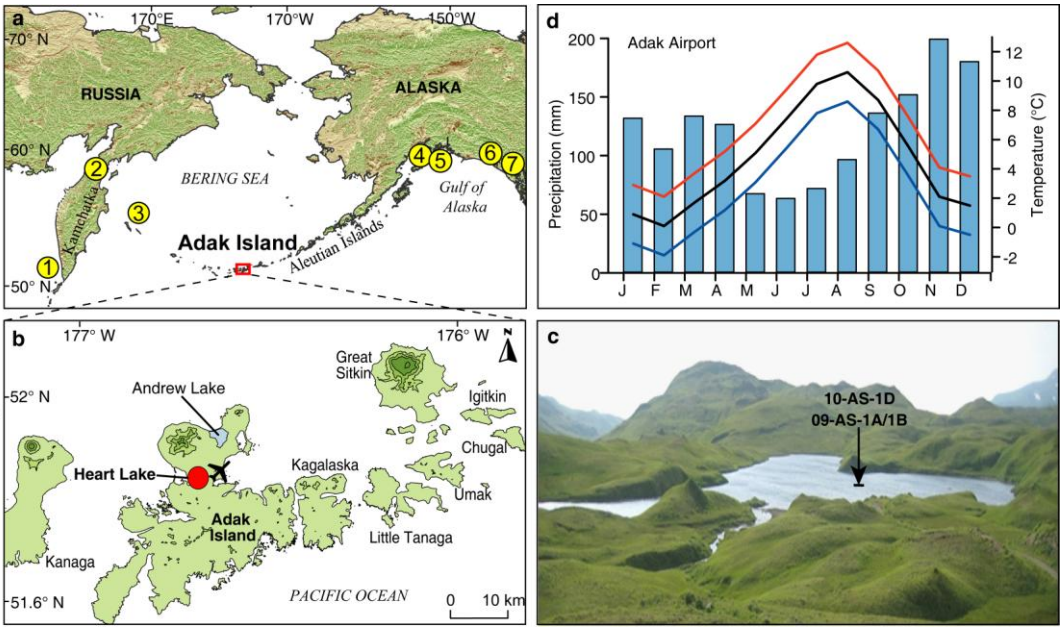

1032

FIG2

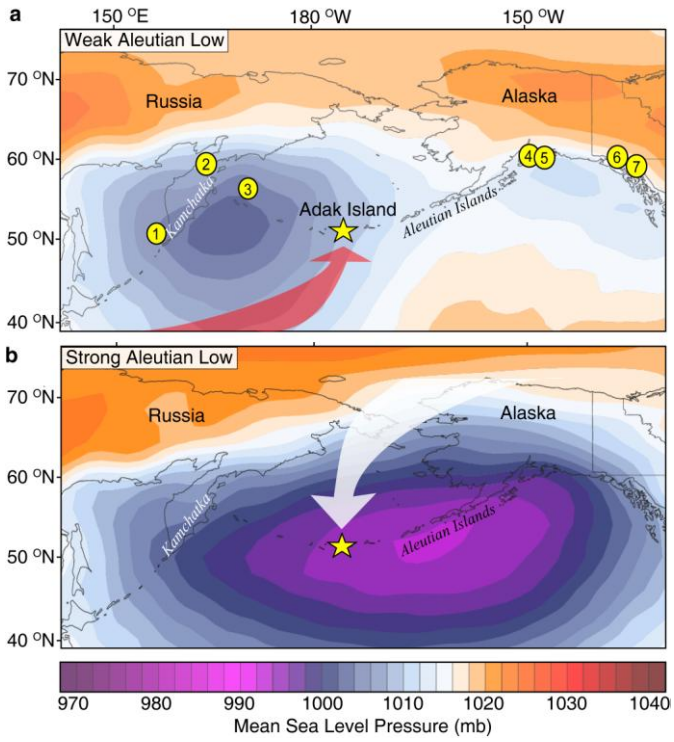

1033

1034

1035

1036

FIG3

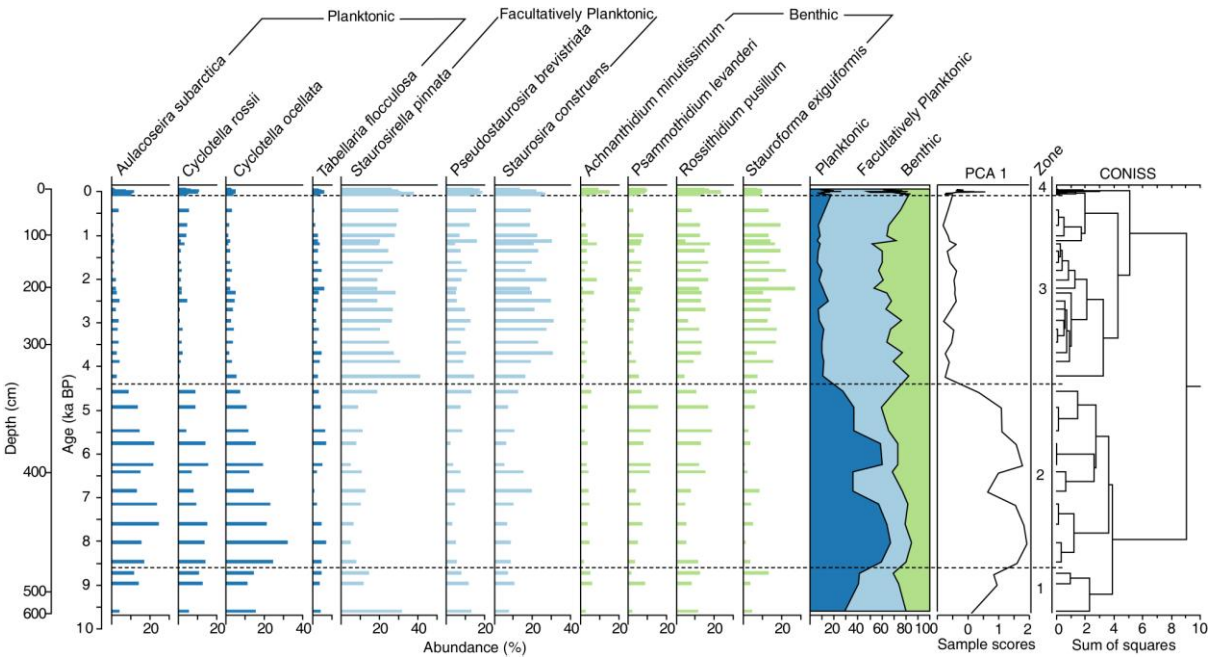

1037

1038

1039

1040

1041 **FIG4**

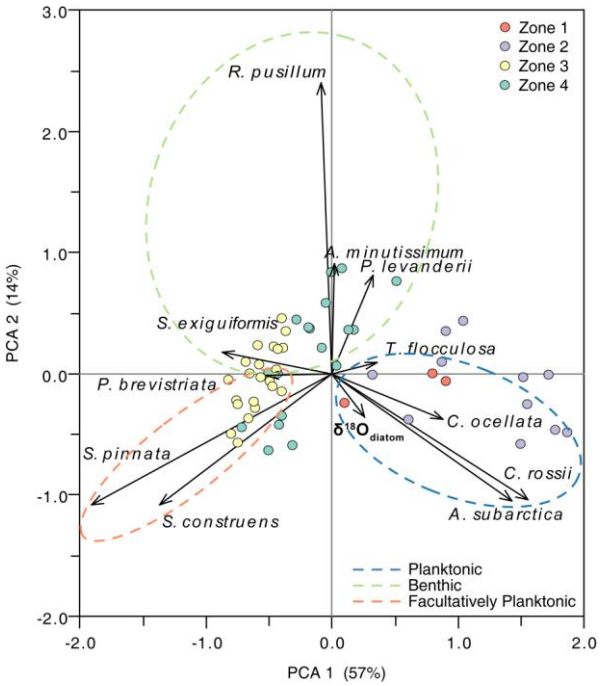

1042

1043

1044 **FIG5**

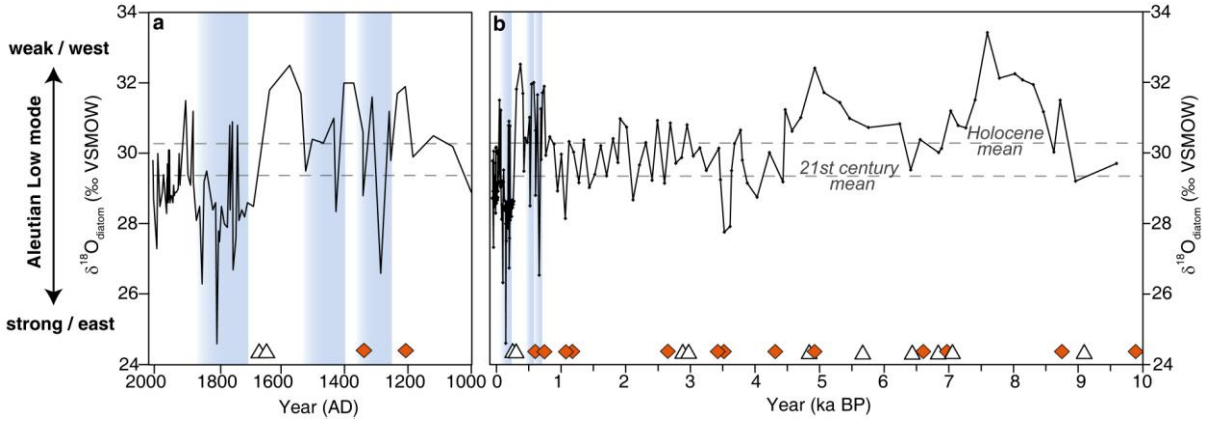

1045

1046

1047

1048

1049

1050

1051

1052

1053 **FIG6**

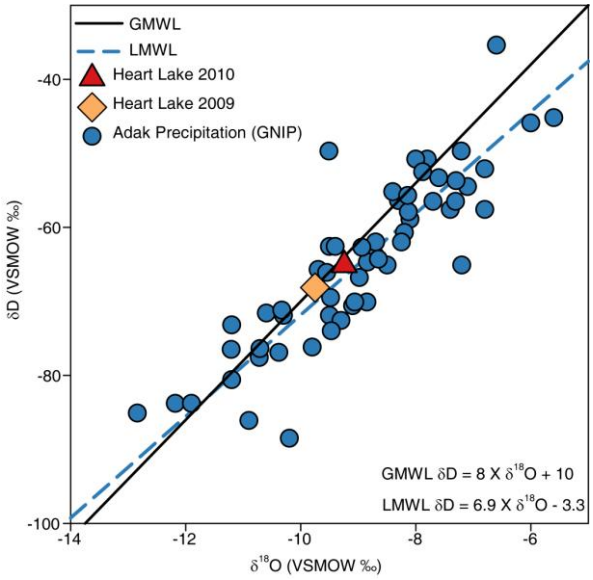

1054

1055 **FIG7**

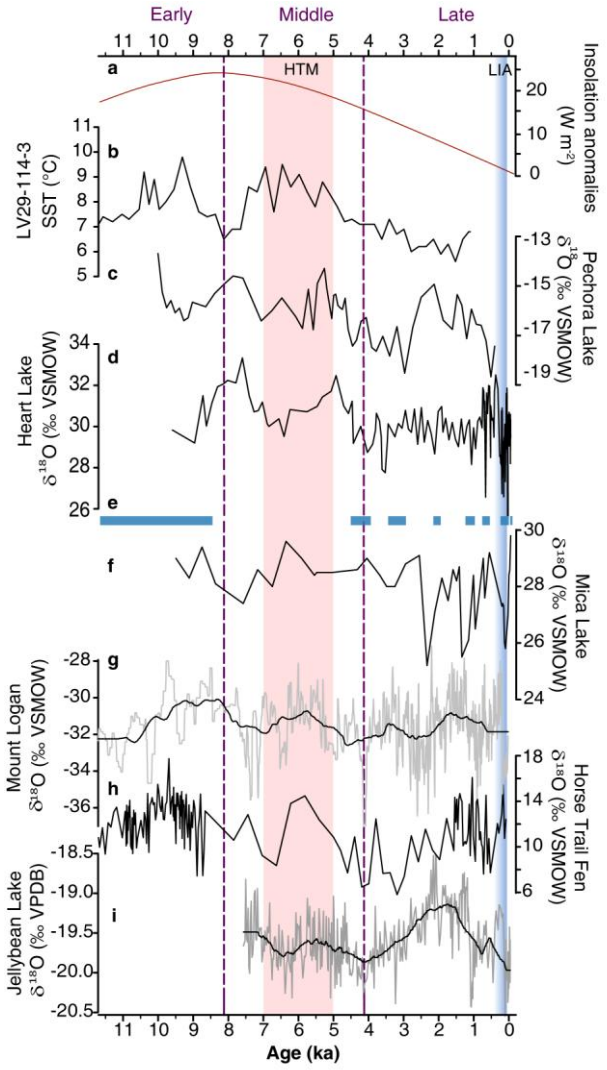
Early
Middle
Late
HTM
LIA
a
b
c
d
e
f
g
h
i
Insolation anomalies (W m^{-2})
LV29-114-3 SST (°C)
Pechora Lake δ^{18}O (‰ VSMOW)
Heart Lake δ^{18}O (‰ VSMOW)
Mica Lake δ^{18}O (‰ VSMOW)
Mount Logan δ^{18}O (‰ VSMOW)
Horse Trail Fen δ^{18}O (‰ VSMOW)
Jellybean Lake δ^{18}O (‰ VPDB)
Age (ka)

1056